Functionalization and processing of porous powders into hierarchically porous monoliths.

Petr O. Vasiliev

Department of Physical, Inorganic and Structural Chemistry,
Stockholm University

Doctoral Thesis in Inorganic Chemistry 2009

Department of Physical, Inorganic and Structural Chemistry
Stockholm University
10691 Stockholm
Sweden

Cover

The front figure represents a schematic overview of the pulsed current processing technique, which was used to produce the hierarchically porous monoliths.

Faculty Opponent

Professor Yoshio Sakka
Nanoceramic Center,
National Institute for Materials Science,
Tsukuba, Japan.

Evaluation Committee

Professor Karin Larsson, Department of Materials Chemistry, Uppsala University.
Professor Xiaodong Zou, Department of Physical, Inorganic and Structural Chemistry, Stockholm University.
Associate Professor Håkan Engqvist, Department of Engineering Sciences, Uppsala University.

Substitute

Professor Åke Bergman, Department of Environmental Chemistry, Stockholm University.

ISBN 978-91-7155-880-0

"It takes all the running you can do, to keep in the same place. If you want to get somewhere else, you must run at least twice as fast as that!"

Lewis Carroll (Through the Looking Glass)

I would like to dedicate this thesis to the people who have helped me.

Abstract

Inorganic porous materials are widely used in a number of applications, where is a need to functionalize and produce materials with a multiscale porosity. The first part of the thesis describes how a novel and facile powder processing approach, using pulsed current processing (PCP) or, as it is commonly called, spark plasma sintering (SPS), has been employed to produce mechanically stable, hierarchically porous bodies from different porous powders.

Surfactant-templated mesoporous spheres were PCP-treated to yield meso/macro porous monoliths. The bimodal pore size can be tailored by choice of templating molecules in the aerosol-assisted synthesis process and by the particle size of the spheres. Diatomite powders were used to produce macro/macroporous monoliths. The densification behaviour of this inexpensive and renewable macroporous raw material was evaluated in detail, and an optimum temperature range was identified where the PCP process yields mechanically strong monoliths.

Binder-less, hierarchically porous zeolite monoliths were produced from various zeolite powders, e.g. silicalite-1, ZSM-5 and zeolite Y. Line-broadening analysis of X-ray powder diffraction data by the Rietveld method and electron microscopy showed that the formation of strong interparticle bonds during the PCP process is associated with a local amorphization reaction that is induced by the high contact stress and temperature. Xylene isomerisation studies showed that binder-less ZSM-5 monoliths display a high catalytic selectivity.

Direct (in-situ) nanoparticle functionalization of surfactant templated mesoporous silica particles has also been demonstrated. Pre-synthesized TiO_2 nanoparticles were dispersed in a precursor solution, containing surfactant and silica source, and processed in an aerosol-generator to produce spherical nanoparticle-functionalized mesoporous particles.

List of publications

The thesis is based on following papers:

I. **Meso/macroporous, mechanically stable silica monoliths of complex shape by controlled fusion of mesoporous spherical particles.** Petr O. Vasiliev, Zhijian Shen, Robert P. Hodgkins, and Lennart Bergström, *Chemistry of Materials*, 18 (20), 4933-4938, **2006.**

II. **Hierarchically porous ceramics from diatomite powders by pulsed current processing,** Farid Akhtar, Petr O. Vasiliev, Lennart Bergström, *Journal of the American Ceramic Society*, 92 (2), 338-343, **2009.**

III. **Forming strong hierarchically porous zeolite monoliths by PCP-induced local amorphization.** Petr Vasiliev, Farid Akhtar, Jekabs Grins, Johanne Mouzon, Charlotte Andersson, Jonas Hedlund and Lennart Bergstrom, *submitted.*

IV. **An X-ray diffraction and gas adsorption study on the effect of pulsed current processing of ZSM-5 and Y zeolites.** Petr Vasiliev, Arto Ojuva, Jekabs Grins, and Lennart Bergström, *manuscript.*

V. **Colloidal aspects relating to direct incorporation of TiO_2 nanoparticles into mesoporous spheres by an aerosol-assisted process.** Petr O. Vasiliev, Bertrand Faure, Boon Sing Ng and Lennart Bergström. *Journal of Colloid and Interface Science,* **2008,** 319(1), 144-151.

Additional publications:

VI. **The radial dependence of the spatial mesostructure of monodisperse mesoporous silica spheres.** Jovice Boonsing Ng, Petr

O. Vasiliev, Lennart Bergström**.** *Microporous and Mesoporous Materials*, **2008**, 112, 589-596.

Patent:

VII. **Zeolite secondary structure**. Petr Vasiliev, Lennart Bergström and Niklas Hedin, patent application.

Table of Contents

1 Introduction

The first subchapter introduces the development and applications of porous materials. The synthesis of mesoporous spherical particles and functionalization of mesoporous materials are introduced in the second subchapter, while the synthesis approaches and applications of hierarchically porous materials are presented in the third subchapter.

1.1 Porous materials

Porous materials are widely used as catalysts, adsorbents, ion-exchange agents and supports because of their high surface area, high activity and open framework structure. Porous materials can be made of inorganic and organic materials and can have a crystalline and quasi-crystalline skeleton (wall) structure. By definition from the International Union of Pure and Applied Chemistry (IUPAC),[1] porous materials can be classified into three groups: microporous (< 2 nm), mesoporous (2 ~ 50 nm), and macroporous materials (> 50 nm), see Figure 1.

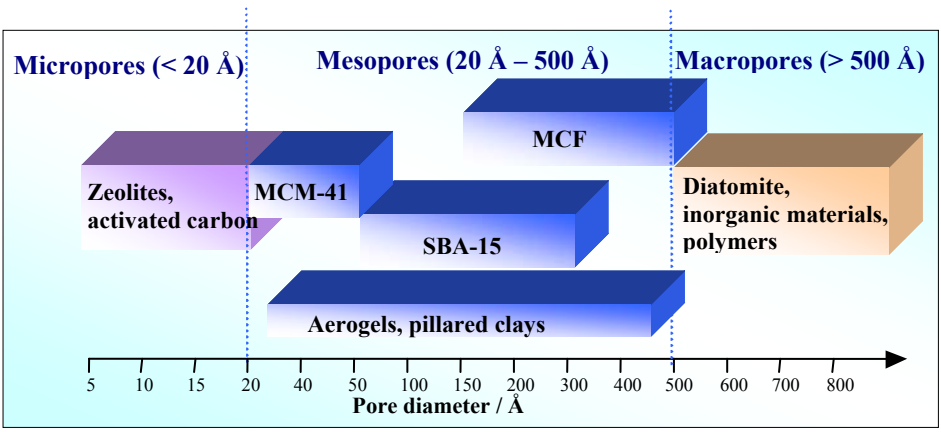

Figure 1. Schematic diagram of porous materials classification by IUPAC with examples of porous materials.

Mesoporous materials are interesting because their pore size is similar to the dimensions of many molecules, which suggests that these materials could be potentially useful in separation and catalytic processes. There are several

examples of mesoporous materials, e.g. pillared clays, porous carbons, and aerogels that have found their use in various applications. During the last two decades, there has been a very large interest in the new types of mesoporous materials with unprecedented long-range order that were independently discovered in Japan (Waseda University) by K. Kuroda and co-workers,[2] and in USA by employees at Mobil Corporation[3-5]. It is worth mentioning that in 1971, a French research group accidentally prepared mesoporous materials with a two-dimensional hexagonal structure similar to MCM-41.[6]

Macroporous materials are abundant in nature, e.g. diatoms, sponges, cork and wood. Macroporous materials with ordered and disordered structures are used in many common applications e.g. as catalyst supports and in water purification, as light-weight structures and in packaging[7, 8]. Macroporous materials also have a potential in new applications e.g. as photonic crystals in light-based information technology[9].

Microporous materials, both in man-made or naturally occurring forms, are widely used in industry for e.g. petro-chemical, adsorbent and detergent applications. Crystalline microporous materials, e.g. zeolites, are characterised by micropores with a high surface area and a specific pore structure that defines the accessibility to the pore cavities. The pore size and pore accessibility together with the chemistry of the active sites on the pore walls determine the specific physicochemical properties, of importance in e.g. catalytic, ion-exchange and sorption applications. Naturally occurring microporous materials are present in different geological formations and include minerals, e.g. clay, micas, zeolites and iron oxides/hydroxides. Synthetic microporous materials include carbon-based materials, e.g. activated carbons,[10] microporous polymers,[11] metal-organic frameworks (MOF)[12] and zeolites and zeolite based materials e.g. aluminosilicates and aluminophosphates.

1.2 Synthesis and properties of mesoporous materials

1.2.1 Synthesis of surfactant templated mesoporous materials

Inorganic materials with ordered mesopores have been prepared using different structure-directing agents, e.g. ionic surfactants, block-copolymers or other self-assembling species.[2-4, 13] The structure and size of the mesopores can be tailored by the molecular architecture of the structure-directing agents, e.g. the length of the hydrophobic domains, and the processing conditions.[14-16] The mesostructured materials are usually synthesized in solution, where the self-assembly and bonding of the amphiphilic molecules with the inorganic precursor species are used to produce materials of various shapes, e.g. thin films,[17-20] fibres[21, 22] and colloidal powders.[21, 23-27]

Several different formation mechanisms have been proposed to describe the synthesis pathway and the interaction between the amphiphilic molecules and the inorganic precursors. Davis et al. suggested that the surfactant molecules self-assemble into rod-like micelles in the aqueous solution and then attach to the inorganic precursor species through specific interactions.[28] The inorganic-organic micelles then spontaneously agglomerate into ordered hexagonal arrays, followed by condensation of the precursors and solidification of the inorganic/organic hybrid material. An alternative cooperative self-assembly mechanism was suggested by Stucky and co-workers, where the charge density matching between organic surfactants and inorganic species controls the formation of ordered structures.[25] Condensation of the silica precursor changes the charge density and induces the formation of ordered phases that consist of both organic and inorganic components.

Reports by Attard et al.[16] and by Ogawa et al.[29] have demonstrated how templated mesoporous silica materials can be prepared by an evaporation driven process. Evaporation of the solvent results in increasing surfactant concentration, which eventually promotes the formation of ordered liquid crystalline phases. Later, Lu et al. prepared thin mesoporous films by evaporation of solvent from a solution containing surfactant at concentrations below the critical micelle concentration (CMC).[17] This process is sometimes termed Evaporation-Induced Self-Assembly (EISA), indicating that the progressively increasing surfactant concentration drives the self-assembly of silica-surfactant micelles and their further organization into liquid crystalline mesophases, see Figure 2.[30] Compared with the “co-operative self-assembly”, where silica species promote liquid crystal phase formation below the CMC (solution precipitation method), EISA can combine the simplicity of the sol-gel

process with the efficiency of surfactant self-assembly, thus allowing rapid preparation of mesostructured colloidal particles, fibres, and thin films with controlled mesostructure. Furthermore, the EISA method provides a general and flexible approach for nanocomposite fabrication by incorporation of non-volatile components, e.g. functional molecules,[31-34] nanoparticles[35] and polymers[36] in the mesoporous matrix.[24]

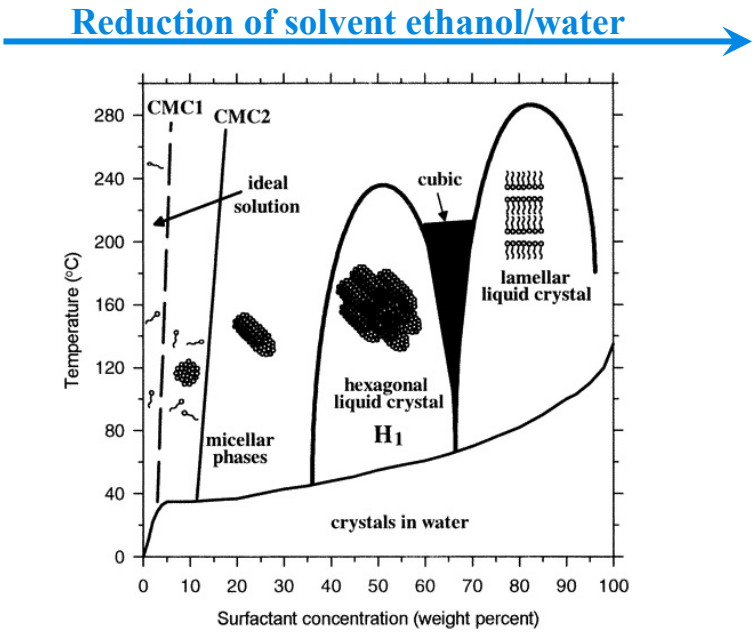

Figure 2. Schematic phase diagram for C_{16}TAB in water. Arrow above the schematic diagram denotes the evaporation-driven pathway during aerosol processing. Adapted from Raman et al.[26]

1.2.2 Functionalization of surfactant templated mesoporous materials

Mesoporous materials have the ability to accommodate molecules[37] or nanoparticles at different sites, e.g. in the pores, onto the walls, or as part of the

solid framework, which is of interest for bio, catalytic and optical applications.[38-43]

Considerable efforts have been made to develop suitable methods for preparing mesoporous functionalized materials utilizing nanoparticle precursors or prefabricated nanocrystals.[44] The nanoparticle precursors can be either introduced into a preformed mesoporous material, e.g. by wet-impregnation[42, 45, 46] or by chemical vapour deposition (CVD)[47, 48], and by directly mixing with a sol-gel mesoporous precursor, to fabricate a mesoporous matrix with dispersed nanoparticles.[45, 49] The functionality and performance of the composite materials formed from precursors are often limited by the difficulty of controlling the composition, size, shape and crystallinity of the in-situ synthesized nanoparticles. It is often preferred to use prefabricated nanoparticles with tailored properties to enhance the performance of the final mesoporous matrix functionalized with nanoparticles. Similar to the precursor-based routes, different nanoparticles can be introduced into the mesoporous matrix e.g. by a wet-impregnation process[50, 51] or directly to the sol-gel mixture[40, 41, 52, 53].

Several attempts have been made to introduce titania nanoparticles into a mesoporous matrix to enhance the photocatalytic performance. Adams et al. synthesized mesoporous silica films with TiO_2 nanoparticles from an acidic silicic acid solution together with a P123 block copolymer.[53] They observed that clustering of nanoparticles in the mesoporous silica film may reduce the available surface area and therefore reduce the efficiency of photodegradation. Inumaru et al. prepared a mesoporous silica composite with a high loading of TiO_2 nanoparticles (up to 60 wt%) by mixing the particles with a C_{16}TAB-containing solution at high pH.[41]

Many applications require that the mesoporous material functionalized with nanoparticles can be dispersed and separated in a liquid or gaseous medium. This is significantly facilitated if the mesoporous material can be produced as powders with relatively narrow size distribution and preferably having a spherical particle shape. Kim et al. showed that magnetic nanoparticles and CdSe/ZnS quantum dots can be embedded into mesoporous silica spheres through a one-pot process.[38] Lu et al. produced mesoporous silica spheres functionalized with Pd nanoparticles in the aerosol-assisted process, by introducing a metal precursor in the precursor solution.[35] Bore et al. reported

how Pt nanowires formed inside the pores of aerosol-produced mesoporous silica spheres by infiltration of an aqueous platinum precursor.[54]

1.2.3 Mesoporous spherical particles

Mesoporous spherical particles can be produced by a controlled growth process using e. g. a modified Stöber process[55] or by conducting the reaction in spherical microreactors, e.g. in oil/water emulsions[56-58].

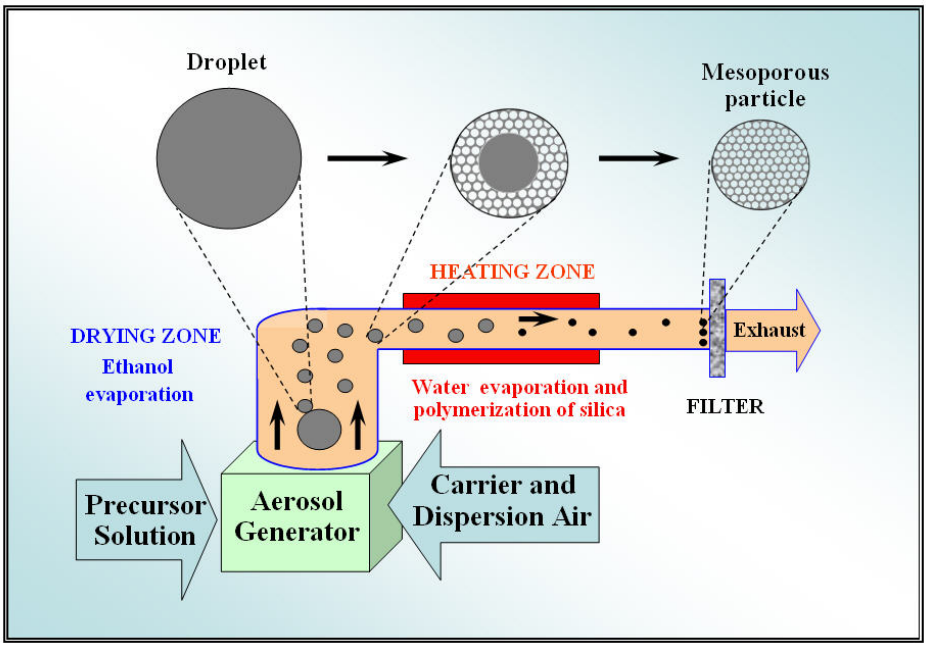

Figure 3. Schematic illustration of the aerosol-based process.

Aerosol-based techniques utilizing the EISA approach have also been used to produce hollow and dense mesoporous particles where the relatively large interfacial tension between the droplet surface and the air yields spherical powders.[21, 23, 59-61] In general, the aerosol atomizer (vibrating orifice or two-fluid nozzle) generates droplets containing the silica precursor, surfactant and solvent, see Figure 3. Solvent evaporation at the gas/liquid interface

enriches the aerosol droplet in surfactant and silicates, resulting in their self assembly into liquid-crystalline mesophases that dynamically grow from the interface towards the interior of the droplet. As the assembling particles pass through the heating zone of the process, further drying and silica condensation result in the formation of mesostructured particles. The surfactant can then be removed by e.g. calcination or dissolution to yield mesoporous spheres.

The first report on an aerosol-based spray drying synthesis of mesoporous particles was published by Bruinsma et al. in 1997.[21] The use of a high drying temperature resulted in the rapid formation of a solid mesostructured crust that yielded mesoporous hollow spheres. Later, Lu et al.[23] demonstrated how non-hollow mesoporous particles could be produced in an aerosol-assisted process by adjusting the evaporation rate to avoid premature solidification of a shell. Later, Andersson et al. presented a modified spraying method with a relatively high yield.[61] Most of the aerosol-assisted techniques produce polydisperse mesoporous particles, but Rao and co-workers showed how monodisperse mesoporous particles could be produced by using a vibrating orifice, which produces monodisperse primary droplets.[59]

1.3 Synthesis and properties of macroporous materials

Various replica, sacrificial template and direct foaming approaches to produce macroporous ceramics have been demonstrated in recent reviews. [7-9, 62-64] Macroporous ceramics can e.g. combine a high permeability with a good mechanical, thermal and chemical stability, which is attractive for a wide range of industrial applications.[65-67] Liquid metal filters of porous alumina,[68] diesel soot filters of alumina and zirconia,[69] and catalyst supports of alumina and corderite[70-72] are examples where porous ceramics already are commercially established, while other applications, including e.g. hard tissue and bone scaffolds, are still in development[73, 74]. The use of porous ceramics in other more mundane, low-cost areas such as wastewater treatment and air purification [75-77] is limited because of relatively expensive starting materials and high energy consumption during production, which is associated with e.g. high processing temperatures.

Diatomaceous earth is an attractive and suitable material for fabrication porous ceramics owing to its low cost, low density and high thermal stability.[78, 79] The source of diatomaceous earth is diatoms, a diverse array of microscopic single-cell algae, who are the most familiar members of phylum Bacillariophyta. The diatoms live in both salt and fresh waters, where they extract silica from the water to build their shells. When the diatoms die, their silica shells accumulate into layers or beds of diatomaceous earth.[80] At present, approximately 1.8 million tons per year of diatomaceous earth are mined worldwide.[81] The chemical composition and the physical structure of diatomite make it of great commercial value for a broad spectrum of applications such as beer filter aids,[77] removal of textile dyes from waste water [82, 83] and sorption of heavy metal ions[84, 85].

1.4 Zeolites

Zeolites are crystalline porous aluminosilicates with pore sizes below 2 nm. The crystal structure defines channels and cages of regular dimensions. Naturally occurring zeolite (stilbite) was described in 1756 by the Swedish mineralogist Baron A.F. Cronstedt. Until the middle of the 20th century, the synthesis of zeolite materials was difficult because of the lack of appropriate analytical techniques. Barrer started the era of synthetic zeolites by synthesising mordenite,[86] and Milton and Breck produced commercially significant zeolites A, X and Y, using inorganic bases in the late 1940s.[86] Ten years later, Barrer and Benny obtained zeolite A with higher Si/Al ratios up to 3 by replacing inorganic bases with organic ones. About twenty years later, researches at Mobil Oil Corp. synthesised new zeolites materials, zeolite Beta and ZSM-5, with higher Si/Al ratios above 5.[87] In 1978 researches at Union Carbide Co. found a way to synthesise silicalite-1, a pure-silica ZSM-5.[88]

The crystal structure of zeolites consists of interconnected AlO_4 or SiO_4 tetrahedra. In the International Zeolite Association (IZA) database are registered more than 190 framework zeolite types (April, 2009), and about 17 of them are used in applications. In addition to the zeolite framework structure, the chemical composition is important and defines some of the specific properties of a zeolite. Generally, an aluminosilicate zeolite formula is

$M_{y/m}^{m+}[(SiO_2)_x \cdot (AlO_2^-)_y] \cdot zH_2O$.

where M corresponds to a cation with a charge *m,* and z depends on the micropore volume. The formula shows that each aluminium ion Al^{3+} introduces a negative charge into the zeolite framework. This charge needs to be compensated by *y*/*m* Me^{m+} cations. As a consequence, zeolites with a high aluminium content are excellent ion exchangers. Furthermore, the aluminium ions act as highly acidic sites that can catalyze a number of chemical reactions. Therefore, the ratio of silicon to aluminium atoms *x*/*y* (or sometimes researches use silica to alumina molar ratio) indicates the content of cations and the number of acidic sites. Zeolites can also be modified by replacing silicon with other element, e.g. Cu, Fe Ge and P, or in a post-synthesis step by incorporating catalytically active metal clusters, e.g. Pt, Fe, or Cu.

The characteristic zeolite properties makes them highly useful in a number of industrial applications e.g. as ion exchangers for water softening, as drying agents or absorbents for organic vapours, as molecular sieves and separation membranes or as catalyst for production of petrochemicals.

Zeolite Y and ZSM-5 are the most frequently used zeolites in catalysis. Zeolite Y is an FAU-type zeolite with a cubic crystal structure. The open pore system consists of spherical cages with a diameter of 1.3 nm which are connected tetrahedrally with four neighbouring cages through windows of 0.74 nm, which results in a three-dimensional, 12-membered-ring pore system. It can be synthesised using inorganic, e.g. Na^+, and organic templates, e.g. crown ethers. ZSM-5 zeolite and its silica analogue, silicalite-1, are MFI-type zeolites with orthorhombic or monoclinic crystal structures. These zeolites have intersecting systems of 10-membered-ring straight and zigzag pores. ZSM-5 is commonly used in the isomerisation of xylenes and the disproportionation of toluene. ZSM-5 can be synthesised in the presence of Na^+ and organic additives, among which tetrapropylammonium cations can be used in a very broad range of experimental conditions.

In catalytic applications, modifications of zeolites (e.g. of pores and also elimination of external sites) are used to optimize the product selectivity and yield. Nicolaides et al. reported on the controlled formation of zeolite materials that have had the crystal structure sufficiently distorted to be called amorphous with a good catalytic performance.[89, 90] Previous work has shown that zeolite amorphization can be induced by different treatments e.g. by subjecting

the zeolite material to heat, ball milling and pressure. Typically, the amorphization results in partial or complete collapse of the porous crystalline zeolite structure, and also in atom migration, e.g. Al. Amorphization of zeolite at temperatures below the melting point has been demonstrated by combining temperature and pressure treatments.[91, 92] The combination of high-energy ball milling and external heating can also result in the formation of crystalline high-temperature phases at relatively low temperature with short heating times.[93-95] Certain zeolites that have been amorphized by intense irradiation have shown an enhancement of the retention capacity of exchangeable ions, which was attributed to the closure of structural channels.[96] This type of materials may be used as back fill material for nuclear waste disposal. [97], [98]

1.5 Hierarchically porous monoliths

1.5.1 Properties and applications

The preparation of hierarchically porous materials that display bimodal porosity e.g. micro/meso-, micro/macro-, meso/macro- porous structures and/or tri-modal porosity with micro/meso/macro- porous structure is a necessary step toward creating porous materials with a high surface area and a low pressure drop for various potential applications in catalysis, adsorption and as support materials. It should be noted that hierarchically porous materials with well-defined macroscopic shapes (e.g. cylinders) are commonly called monoliths in the scientific literature, but usually pellets, granules and secondary structures in the patent literature. In e.g. the catalysis area the term “monolith” is specifically used to describe cylinders with macroporous channels.

For many applications, the size of the porous particles is too small to be convenient in practice. Common problems relate to dusting, handling, filling, productivity losses because of clogging and excessive pressure drops, recovery, and inactivation. Hence, catalyst and adsorbent applications require that the porous material is available in macroscopic form, e.g. granules, pellets or monoliths.[99-102] Common approaches to produce hierarchically porous materials involve the use of a combination of structure-directing agents that control the structure at different length scales, or controlled phase separation in a confined space.[103, 104]

The current technology for producing e.g. zeolite monoliths for catalytic and adsorbent applications involves extrusion or pressing zeolite crystals (particles) together with a non-zeolitic binder, followed by a drying and heating step.[100] The non-zeolitic binders are usually added to impart high mechanical strength and resistance to attrition of the zeolite granules or pellets. Examples of suitable inorganic binders include materials such as alumina, silica and various types of clays. [105]

Several attempts to minimize or eliminate the use of non-zeolitic binders have been reported. The concept of binder-free zeolite (without common binders like alumina and clays) was introduced by Bowes, where a self-bound zeolite was prepared by mulling, extrusion and drying a mixture of ZSM-5 zeolite powder together with a hydrated silica and sodium hydroxide in water.[106] Different zeolites prepared following this procedure showed almost an order of magnitude reduced aging rates in catalytic dewaxing processes, and side reactions catalyzed by a binder were eliminated.[107] Later, Verduijn showed that silica binders may be converted into a wide variety of zeolite crystal structures, by aging the silica/zeolite composite in an ionic solution.[108] Recently, zeolite-bound zeolite catalyst have been prepared by e.g. hydrothermal transformation of the non-zeolitic binder using zeolite seeds. [109], [110] Dong et al. reported how multiporous zeolite monoliths can be produced by hydrothermal transformation of mesoporous silica spheres coated with zeolite particles.[111]

1.5.2 Templated synthesis

Alternative routes for shaping hierarchically porous materials in macroscopic form have also been attempted. Monoliths with hierarchical pore structure were produced using zeolite particles as building blocks organized around templates, e.g. foams or carbon aerogel. Tao et al. prepared multiporous ZSM-5 monoliths by the templating method, using carbon aerogels of uniform mesoporosity.[112, 113] Lee et al. synthesised monolithic ZSM-5 zeolite foams by utilization of polyurethane foams as template.[114, 115] Also, Tong et al. synthesized monolithic zeolite beta with multiporous structure, using carbon as a transitional template.[116] Trimodally porous monoliths were prepared using

mesoporous particles as building blocks together with a polyurethane foam as macrotemplate.[117] Starch gel templates together with zeolite nanoparticles have been used to fabricate hierarchical micro/meso/macropore monoliths.[118]

Hierarchical porous materials can also be prepared by mixing the different templates and the inorganic precursors in a one-step procedure. Haskouri et al. prepared bimodally porous monoliths in a one-step surfactant-assisted procedure by using a C_{16}TAB templating agent for mesopores and controlling synthesis and ageing conditions so as to form large pores.[104] Maekawa et al. prepared meso/macroporous monoliths from polymer foams in a two-step procedure in which a moulded polystyrene foam serves as a macroporous precursor scaffold for the mesostructure-forming sol-gel/amphiphilic block copolymer composite.[119] Through careful control of pH in a sol-gel process, Morales et al. controlled the packing of aggregated nanoparticles to produce a material with a bimodal pore systems.[120] Lee et al. produced silica foams with ordered mesopores and mesocellular pores by using a single structure-directing agent (tri-block copolymer).[121] Latex particles, a block copolymer and an ionic liquid were used as templates by Kuang et al. to produce trimodally porous material.[122] Anderson's group produced a hierarchically porous material (macro-, meso- and microporosity) by mixing latex spheres and block copolymers.[123] However, solution-based templated synthesis techniques to control the pore structure and prepare the monoliths suffer some inherent problems. Removal of large amounts of solvent from large objects with high porosity and small pore sizes is very time consuming, with processing times usually on the order of several days.

Controlled phase separation and gel-casting have also been used to produce hierarchically porous monoliths. Smått et al. used controlled phase separation and gelation kinetics with surfactant to prepare trimodally porous monolithic bodies.[124] Liang et al. produced silica columns with a well-defined mesopore and tunable macropore structure by gel-casting of pre-synthesized mesoporous particles.[125] Other approaches, involving controlled phase-separation in parallel with sol-gel transition of the inorganic precursor,[103, 126] have also been successful in creating hierarchically porous monoliths.

1.5.3 Powder processing routes

Powder processing is the preferred method of producing ceramic materials.[127] Powder processing consists of the following steps: powder synthesis, assembly of the powder to an engineering shape, removal of all organic additives, and finally sintering to give the material sufficient mechanical strength. The most common method to shape a powder body is dry pressing, where a mould or die is filled with powder granules that commonly contain organic additives, e.g lubricants and binders. The granules are then compressed between punches in a die to form what is called a 'green' compact. The powder compact produced is then heated to remove all organic additives before the powder body is sintered by heating at a high temperature, sometimes under pressure for a prolonged time. The process of sintering is used to produce dense objects of a wide variety of materials, e.g. ceramics such as alumina and silicon nitride and brittle metals with high melting temperatures (over 3000K), such as tungsten. Components of various shape and size can be manufactured by powder processing routes: these can range from bathroom sinks for domestic applications to the insulating sleeve in a spark plug.

Materials have been produced by sintering for several thousand years. One of the earliest examples of sintering (about 6000 BC) is the formation of bricks by heating clay bodies in an open pit fire used by the Mesopotamians.[128] The Egyptians sintered metals and ceramics already before 3000 BC.

By definition, sintering is a process where heating a powder body induces mass transport to the regions of a lower surface free energy, e.g. particle necks with a negative curvature. Sintering of powder compacts results in improved mechanical strength and reduced porosity. There are different types of sintering, e.g. pressure-less sintering and hot-pressing. Invariable, these processes rely on the use of an externally heated furnace where the heat is mainly transferred by convection and radiation.

In the early sixties, Japanese researches designed a process where an applied electric current induced the necessary temperature increase to sinter various powders.[129, 130] Several companies produced machines based on this invention during the 1980´s, which spurred a significant interest from both the academic and industrial community.

The process relies on the use of an electrically conductive die made of e.g. graphite, where the Joule heat creates a rapid temperature increase. In addition, depending on the electrical resistance of the powders, some of the applied electric current may also pass through the powder body and directly heat the material. The technique typically utilizes on-off DC pulses and a simultaneously applied uniaxial pressure in order to facilitate sintering to produce dense ceramics. The detailed understanding of the process is still a topic of intense debate, and claims of spark discharges, electrical fields and Joule heating at points of high temperatures in areas between particles are speculations that need to be investigated in detail. Because of the rapid heating rates, materials processing is complete within short periods of approximately 30 minutes. The possibility to process materials at comparably low temperatures combined with short processing times enables tight control over grain growth, microstructure and densification.

During the last two decades, the interest in electric current-driven heating and sintering has increased significantly. Various commercial manufacturers try to advertise their machines with specific trade names for the process, e.g. plasma assisted sintering" (PAS), "Field assisted sintering technique" (FAST), "and "spark plasma sintering" (SPS). We prefer to use the more neutral term "pulsed current processing" (PCP) that solely relates to the process without indicating a specific brand of machine or an assumption about the nature of the process.

In the ceramic field, pulsed current processing is often used to produce dense nanostructured materials, e.g. ceramics, glasses and alloys. The problem of grain growth in conventional sintering methods can be overcome because of high heating rates, lower sintering temperature and shorter holding time.[131] Indeed, PCP can also be used to produce partially sintered porous materials from different powders. There are reports on the preparation of porous materials using PCP of e.g. alumina,[132] stainless steel[133] and macroporous calcium phosphate scaffolds[134].

2 Objectives.

1. Development of a novel approach to producing hierarchically porous monoliths.

The main objective was to investigate how a novel powder processing method, the pulsed current processing (PCP) technique, could be used to produce hierarchically porous monoliths.

More specifically, we were interested in evaluating this technique for various types of porous powders e.g. powders where the pore size and the amorphous or crystalline nature of the solid material is varied.

We also wanted to understand how the material responds structurally to the PCP treatment.

2. Development of a versatile route to functionalizing mesoporous spheres with nanoparticles.

The main objective was to develop a new method of direct nanoparticle functionalization of mesoporous particles in an aerosol assisted process.

We also wanted to understand the colloidal stability of nanoparticles in a precursor solution in order to successfully produce functionalized mesoporous particles.

3 Experimental

3.1 Synthesis of spherical mesoporous silica particles with and without incorporation of TiO_2 nanoparticles.

3.1.1 Polydisperse mesoporous particles

Polydisperse mesoporous particles with an internal pore size of 96 Å, were produced by a modified spray-drying technique using a two fluid nozzle [61] (supplied by the Institute for Surface Chemistry (YKI)).

3.1.2 Monodisperse mesoporous particles

Monodisperse mesoporous spheres were produced using a vibrating-orifice aerosol generator. Water- and ethanol/water-based[61] solutions were used to produce mesoporous spheres with and without incorporation of TiO_2 nanoparticles via the aerosol assisted technique. The amount of ethanol was experimentally optimized to produce spherical monodisperse particles by using the vibrating orifice.

The prepared solutions were introduced into the aerosol generator. The operation of the aerosol generator is based on the instability and breaking up of a cylindrical liquid jet via a vibrating orifice (20 μm and 35 μm) into uniform droplets.[135] A pump syringe (velocity from $1.3 \cdot 10^{-3}$ to $4.4 \cdot 10^{-3}$ cm/s, depending on the orifice diameter) forces the precursor solution through the vibrating orifice (70-80 kHz, should be adjusted to avoid formation of satellite droplets) at constant speed, therefore creating droplets of relatively uniform diameter, Figure 4. The droplets were injected axially from the vibrating orifice with a turbulent dispersion air jet (~15 ml/min) to suppress any coalescence of droplets, followed by a greater volume of a lamellar flow of dilution air (~ 40 L/min) into a vertical drying-chamber (10 cm diameter) where evaporation of solvent takes place, Figure 4. As the surfactant concentration reaches or exceeds its CMC, self assembly of the surfactant molecules occurs (EISA), forming the template for the hydrolyzed silica source. The silica condensation is enhanced

by passing the particles through a stainless steel tube (4 cm diameter) inside a three-zone furnace at 250°C (calibrated with thermocouples) before the particles are collected on a filter (Pall, A/D Glass fiber filter, with diameter 4.7 mm and pore size 3 μm). The C_{16}TAB or P123 templated mesoporous particles were calcined at 550°C for 4 hours in air to remove the surfactant template.

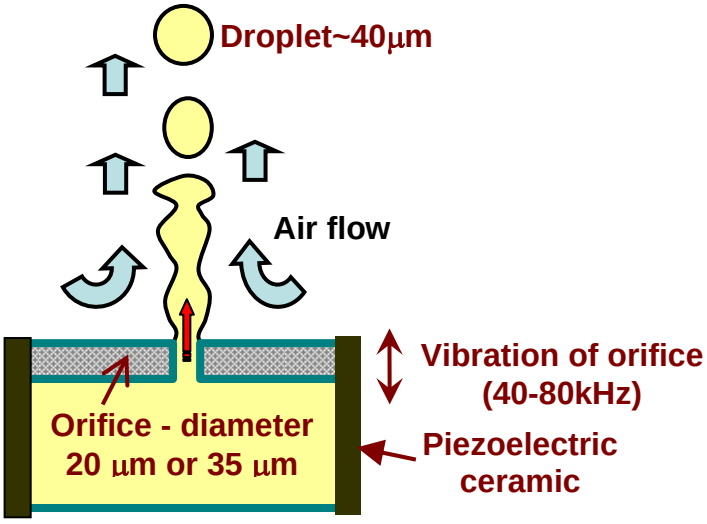

Figure 4. Schematic diagram of the break-up of a cylindrical liquid jet by a vibrating orifice to produce monodisperse droplets.[136]

3.2 Pulsed current processing of porous powders

Hierarchically porous monoliths have been fabricated from porous particles (mesoporous, diatomite and zeolite are described below) using a pulsed current processing apparatus (Dr. Sinter 2050, Sumitomo Coal Mining Co. LTD, Japan), see Figure 5. Porous particles were loaded in a graphite die (typically with cylindrical shape) which was placed into the vacuum chamber of the PCP apparatus. The powders were processed at a typical heating rate of 100°C/min and a uniaxial pressure of 20 MPa. The rapid temperature increase is created by the on-off DC pulse voltage and electric current that is passed through the graphite die and the powder assembly to generate Joule heat.

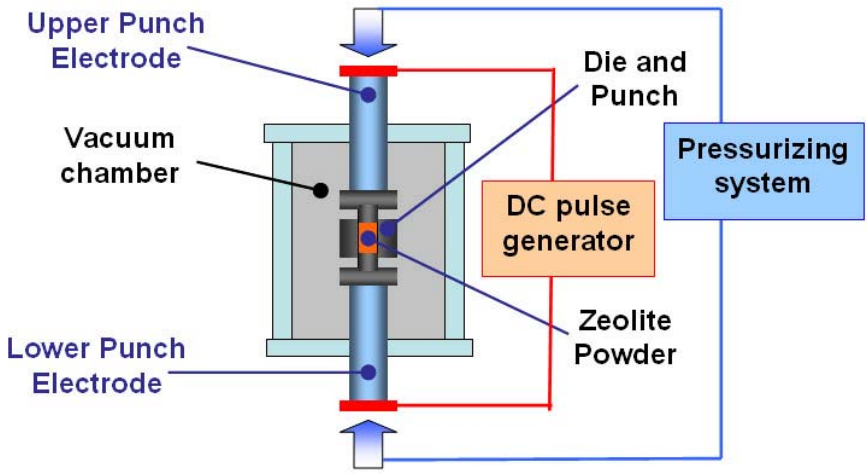

Figure 5. Schematic diagram of the pulsed current processing apparatus used to produce porous monoliths.

3.2.1 Mesoporous particles

The mesoporous polydisperse particles were produced following the procedure described in section 3.1.

3.2.2 Diatomite macroporous powders

The diatomite powders were obtained from Qingdao Tosens Diatomite Co. Ltd and were melt aid calcined at 900°C and have an average particle size of 5 μm.

3.2.3 Zeolite microporous powders

The zeolite ZSM-5 powders with molar ratios of SiO_2/Al_2O_3 = 280 (CBV 28014) and zeolite Y with molar ratios of SiO_2/Al_2O_3 = 60 (CBV760), SiO_2/Al_2O_3 = 30 (CBV720) were obtained from the Zeolyst International company.

The silicalite-1 powder was prepared at Luleå Technical University by first adding 5.29 g of a solution of tetrapropylammonium (TPAOH: 40wt% solution, Applichemie) and then 7.81 g of precipitated silica (Merck) to 20.25 g of distilled water until a homogeneous gel was formed. The mixture was subsequently transferred to a Teflon-lined autoclave, and hydrothermal treatment was carried out at 170°C under autogenous pressure for 24 hours. The obtained particles were purified by repeated filtration (Munktell 00H filter paper) and washed with distilled water. After drying the resulting cake at 110°C for 12 hours, the powder was gently disagglomerated in a mortar and calcined for template removal in a tubular furnace at 500°C for 8 hours (heating rate 1°C/min, cooling rate 1.5°C/min) under flowing oxygen (100mL/min). The resulting powder was confirmed to be silicalite-1 by XRD and consisted mostly of twinned crystals of about $10\times10\times14$ μm^3 with narrow size distribution.

3.3 Characterization

Characterization of the porous materials was carried out using the following methods and corresponding equipment.

3.3.1 Structure, composition and morphology

Scanning electron microscopy (SEM) micrographs of mesoporous particles and monoliths were obtained with a JEOL 820 microscope. SEM micrographs of diatomite and zeolite particles and monoliths were obtained with a field emission scanning electron microscope (FE-SEM) JEOL JSM-7000F. Representative cross sections have been obtained using a JEOL SM-09010 cross section polisher operated at 6 kV for 7 hours.

Transmission electron microscopy (TEM) micrographs were taken with a JEOL JEM-200 FX-II microscope operating at 200 keV, equipped with a CCD camera. Samples were ground before being dispersed in ethanol, and were then deposited onto a carbon film supported on a Cu grid. Also, powders were microtomed to get ultrathin sections of mesoporous particles. First, the mesoporous particles with TiO_2 nanoparticles were embedded directly in an epoxy resin, Spurr, that was polymerized at 70°C for 16 hours. Then, ultrathin sections (thickness about 70 nm) were cut on Leica Ultracut UCT equipped with

a Drukker diamond knife, and the sections were picked up on Cu grids with a pioloform film.

The elemental composition of the diatomite monoliths and mesoporous particles functionalized with TiO_2 nanoparticles was determined with an Energy Dispersive X-ray Spectrometer (EDS, Link system AN 10000).

Powder X-ray diffraction (PXRD) patterns of the calcined mesoporous/macroporous bimodal monoliths were obtained using a STOE powder diffractometer using CuK_α radiation. X-ray powder patterns of diatomite and zeolite powders and corresponding grinded powders of consolidated monoliths were recorded using $CuK\alpha_1$ radiation (λ = 1.5406 Å) and a PANalytical X´pert PRO MPD diffractometer equipped with a Pixel detector. The measurements were carried out using 16 mm diameter reflection mode holders, variable slits with a constant area of one square cm irradiated, a continuous scan mode with step size 0.0131°, the 2θ range 7-100° and a total measuring time of 144 min, yielding patterns with maximum peak intensities of *ca.* 17000.

Size and strain analysis from X-ray powder diffraction peak broadenings[137, 138] was made by the Rietveld method, using the program FullProf[139]. In the analysis, the Thomson-Cox-Hastings pseudo-Voigt function was used, with Lorentzian and Gaussian component peak half-widths of respectively $H_L = X\cdot\tan(\theta) + Y/\cos(\theta)$ and $H_G^2 = U\cdot\tan^2(\theta) + V\cdot\tan(\theta) + W + I_G/\cos^2(\theta)$, and assuming that size broadening is described by terms having a $\tan(\theta)$ dependence, *i.e.* X and $U^{1/2}$, and strain broadening by terms having a $1/\cos(\theta)$ dependence, *i.e.* Y and $I_G^{1/2}$. Lorentzian and Gaussian components for the instrumental resolution were estimated by measurements on a sintered NIST standard alumina disc, giving peaks with a Gaussian component above 85% and half-widths of respectively *ca.* 0.05 and 0.10° at 20° and 100°. The peak widths for the ZSM-5 starting material were respectively *ca.* 0.07 and 0.24° at 20° and 100°. The peak widths for the consolidated samples were larger, showing a progressive peak broadening with increasing consolidation temperature. In the refinements, the determined resolution function was specified and the parameters V and W set to zero, and the parameters U, I_G, X and Y refined. For the zeolite ZSM-5 samples the parameters U, I_G, X and Y were all refined, while for the zeolite Y samples, which exhibited nearly pure Lorentzian peak shapes, only X and Y were refined. The background was refined by using *ca.* 5

polynomial coefficients and *ca.* 4 Debye-like functions. Atomic coordinates for ZSM-5 (space group $P2_1/n$) were taken from the single crystal structure determination of dehydrated ZSM-5 with composition of $[H_{0.32}][Si_{95.68}Al_{0.32}O_{192}]$ by van Koningsveld *et al.*.[140] Atomic coordinates for zeolite Y (space group $Fd\text{-}3m$) were taken from the database of International Zeolite Association and were refined. The final residual χ^2 values for the refinements varied between 1.2 and 3.2, and the R_F values between 2.1 and 3.7%.

3.3.2 Porosity

Nitrogen adsorption/desorption isotherms were obtained volumetrically with a micromeritics ASAP 2020 analyzer. Samples were degassed and data collection started at typically 77 K, following a program consisting of both an adsorption and a desorption branch. The specific surface areas were calculated using the Brunauer-Emmett-Teller (BET) model.

The macropore volume and the median pore size distribution in the interval $3\ \text{nm} \leq \Phi \leq 360\ \mu\text{m}$ were determined using mercury intrusion porosimetry (Micromeritics AutoPore III 9410). The surface tension and the contact angle of mercury were set to 485 mN/m and 130°, respectively.

3.3.3 Mechanical stability

The monolith's mechanical stability was evaluated using the diametral compression test (also known as Brazilian disc test or splitting tensile test) on cylindrical monoliths prepared at different temperatures. This simple test, which is frequently used to characterize powder bodies and composites,[141] subjects a circular disk to a compressive stress between two diametrically opposed plates until a crack forms, causing failure of the specimen (Figure 6). The strength of the material can be related to the tensile stresses that develop perpendicularly to the loading direction and are proportional to the applied compressive force.[142] Diametral compression tests were carried out at ambient conditions using an electromechanical testing machine (Zwick Z050, Germany) at a constant cross-head displacement rate of 0.5 mm/min. Tensile strength is

calculated as $\sigma_T = 2P/d \cdot t \cdot \pi$, where P = load at failure (N), d = specimen diameter (mm) and t = specimen thickness (mm).

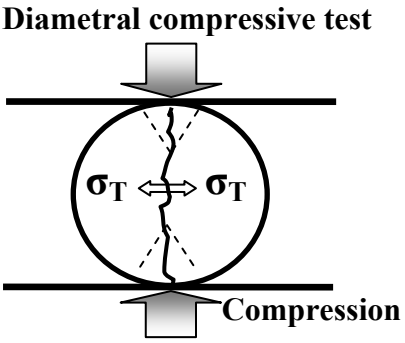

Figure 6. Outline of the tensile strength measurement by diametral compression test.

3.3.4 Catalytic activity

A tubular stainless steel reactor was used for the catalysis experiments. The internal diameter and length of the reactor were 17 mm and 200 mm, respectively. The zeolite samples were mixed with 90 wt% acid-leached sea sand and ethanol and stirred for 20 minutes until a homogenous mixture of zeolite and sand was obtained. The sand is inert at the reaction conditions. The lower portion of the reactor was first loaded with (inert) glass beads, and the zeolite/sand mixture was subsequently loaded in the middle of the reactor. Finally, the upper portion of the reactor was filled with glass beads. Glass wool barriers were used to prevent the zeolite/sand mixture and the glass beads from moving in the reactor. The zeolite pellets were ground for 5 minutes in an automatic mortar grinder (Fritsch Pulverisette 2). The mortar was cleaned by repeated grinding of sea sand before grinding the pellets. The original zeolite powders and ground pellets were heated in a furnace at 500ºC for 6 hours, with a heating and cooling rate of 0.2ºC/min to obtain the H^+ form. The samples were calcined in-situ at 450ºC for 6 hours prior and in between testing. The feed and the products were analyzed with a gas chromatograph (Varian CP 3800) with a polar column (CP Xylene, vendor) and a flame ionization detector (FID) connected on-line.

4 Results and Discussion

In part 4.1 a novel approach to producing hierarchically porous monoliths is presented. Using different porous powders, it was shown that hierarchically porous monoliths can be produced with different porous hierarchies i.e. macro/macro, meso/macro and micro/meso/macro porosities by the PCP technique. The monoliths have a well-defined shape and high mechanical stability.

In part 4.2, the preparation of monodisperse mesoporous particles and the functionalization with TiO_2 nanoparticle using an aerosol-assisted process are summarized.

4.1 Hierarchically porous monoliths

Pulsed current processing is a novel processing technique that is frequently used to produce dense ceramic materials. Here, we employed the pulse current processing technique to produce hierarchically porous bulk materials directly from porous powders.

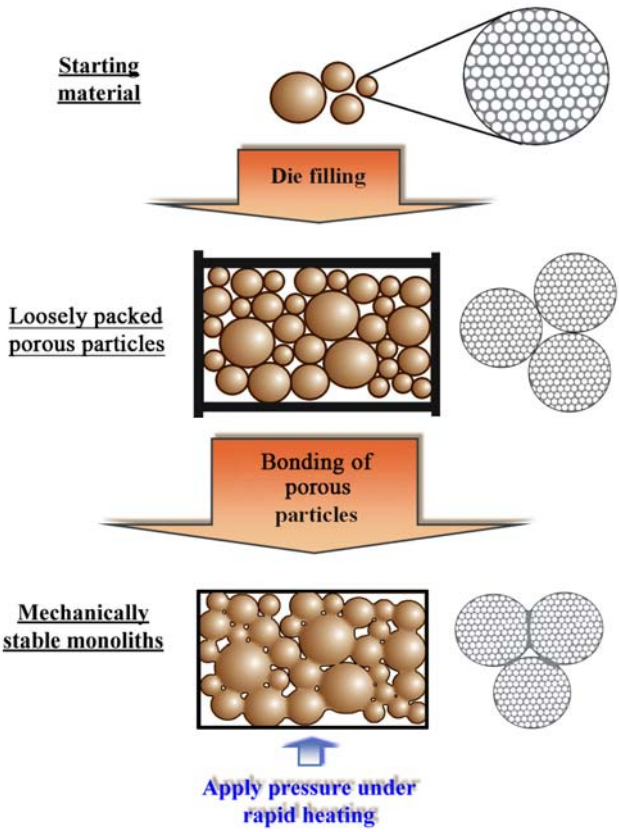

Figure 7. Schematic illustration of the process used to prepare porous monoliths from porous particles: mesoporous, diatomite and zeolites.

The rapid and facile approach used to produce mechanically stable porous monoliths from different porous particles is schematically illustrated in Figure 7. It involves three steps, namely: (*i*) synthesis of porous particles; (*ii*)

assembling the particles in a die with a designed shape; and (*iii*) subjecting the powder assembly to a pulsed current in a die and simultaneously applying a compressive stress.

The primary objective of our study is to produce mechanically stable hierarchically porous monoliths. Hence, the consolidation process is restricted to the initial stage, where mass transport is insignificant and the pores inside the used material are preserved. Pulsed current processing (PCP) offers the advantages of a high heating rate, which makes the total heating time short, and the possibility of simultaneously subjecting the powder assembly to a compressive stress.

4.1.1 Meso/macro porous monoliths

Hierarchically porous monoliths with a bimodal meso/macro-porous structure were produced by the PCP technique, using two different mesoporous powders. The major part of the work is based on polydisperse mesoporous silica spheres (with diameters in the range of 0.5 - 5 μm) produced by a recently reported spraying technique, see Figure 8a.[61] Monodisperse mesoporous particles (Figure 11a) with a diameter of 12 μm were also used. This powder was produced with a vibrating orifice aerosol generator.

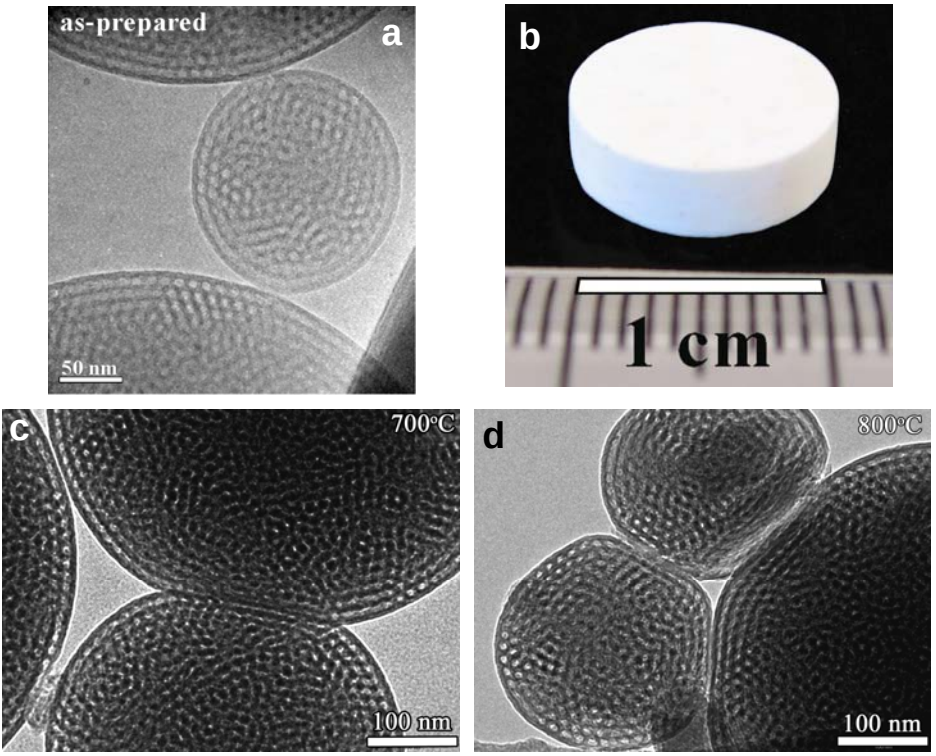

Figure 8. a) TEM micrograph of polydisperse mesoporous silica particles; b) photograph of silica monolith made of the mesoporous particles produced by PCP at 700°C and 20 MPa; c) and d) TEM micrographs of the deformed contact zone of the mesoporous particles PCP at 20 MPa and 700°C and 800°C, respectively. The mesoporous particles were prepared by a modified spray drying process of an acidic ethanol solution of hydrolyzed TEOS and the triblock copolymer P123.

Figure 8b shows that monoliths can be produced by rapidly heating the mesoporous particle assemblies and simultaneously subjecting the powder body to a compressive stress. This process is able to deform and fuse the silica particles together at the contact points, as illustrated in Figure 8c and d. The TEM images suggest that the high stress at the contact points at PCP maximum temperatures (T_{PCP}) above 650°C results in a viscoelastic deformation of the amorphous silica framework. It is well known that this type of amorphous, glass-like material (on the atomic length-scale) exhibits a time-dependent deformation behaviour also below the glass transition point.[143, 144] Figure 8c suggests that at T_{PCP} of 700°C this deformation results in the formation of a relatively small contact zone. Increasing the temperature to 800°C results in a larger deformation of the particles, which also appears to distort the mesostructure, at least in the region close to the deformation zone, Figure 8d.

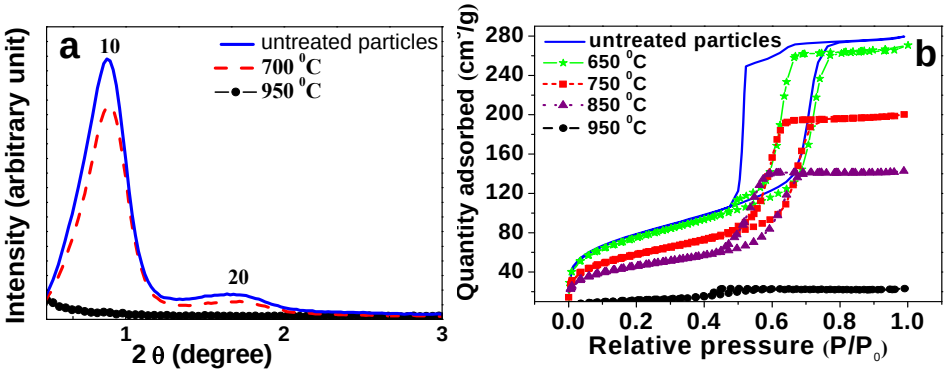

Figure 9. a) Small-angle X-ray diffraction of the untreated polydisperse mesoporous particles and PCP treated at 700°C and 950°C; b) N_2 isotherms of untreated and PCP treated polydisperse mesoporous particles at temperatures between 650°C and 950°C. The mesoporous particles were prepared by a modified spray drying process of an acidic ethanol solution of hydrolyzed TEOS and the triblock copolymer P123.

The TEM micrograph (Figure 8a) of the polydisperse mesoporous particles indicates the presence of only relatively small 2D hexagonal domains. The XRD data of the untreated P123-templated polydisperse particles and the monoliths processed at T_{PCP} of 700°C display nearly identical patterns, which suggests that

there is no degradation of the internal mesostructure induced by the PCP-treatment at this relatively low temperature, Figure 9a. The positions of the two main peaks, 10 and 20, observed in the XRD patterns of particles correspond to the unit cell parameter a = 116 Å with corresponding d-values of 100 Å and 50 Å. Previous reports on the aerosol-generated mesostructured particles have also shown a similar structure.[61] At a T_{PCP} of 950°C or higher, the peak reflections characteristic of the obtained mesostructure are not observed, indicating collapse of the mesostructure within the particles (Figure 9a).

Maximum temperature (T_{PCP}) (°C)	**Specific surface area[(a)] (m^2/g)**	**Total pore volume[(b)] (cm^3/g)**	**Total macropore volume[(c)] (cm^3/g)**	**Tensile strength[(d)] (MPa)**
1050	**2.28**	**0.0015**	**<0.01**	**-**
1000	**2.56**	**0.003**	**-**	**23.8**
950	**38**	**0.035**	**0.18**	**-**
900	**147**	**0.191**	**-**	**7.4**
850	**159**	**0.219**	**0.19**	**-**
800	**191**	**0.296**	**-**	**1.6**
750	**202**	**0.307**	**0.26**	**-**
700	**239**	**0.368**	**-**	**0.8**
650	**261**	**0.411**	**0.32**	**-**
as-made	**275**	**0.429**	**-**	**-**

Table 1. Porosity and tensile strength of PCP treated polydisperse mesoporous particles at different T_{PCP}.

[(a)]BET surface area calculated within $p/p^0 = 0.08 – 0.3$.

[(b)] Single point total pore volume calculated at $p/p^0 = 0.96$.

[(c)] Macropore volume for all pores with a diameter above 0.1 μm.

[(d)]Tensile strength was obtained from diametral compression test of cylindrical monoliths.

The shapes of the N_2 adsorption/desorption isotherms (Figure 9b, Table 1) are typical for mesoporous solids with cylindrical pore geometry. We have estimated the mesopore diameter using the NLDFT model.[143] The untreated mesostructured spherical particles have a pore size of 96 Å. This pore size is retained when the T_{PCP} is 700°C, while slight reductions in the pore size to 82 Å and 75 Å are observed for monoliths treated at T_{PCP} of 750°C and 800°C, respectively. Both the specific surface area and the volume of the mesopores decrease with an increase of PCP temperature (Table 1). The decrease appears to be linear from 650°C up to 950°C where the mesostructure collapses. This suggests that the mesopore size of the monoliths is very little affected by the pulsed current processing up to at least 800°C. The viscoelastic deformation at the contact points of the spherical particles only results in a local elimination of the pores. Hence, keeping the T_{PCP} to 700°C or less, it is possible to prepare meso/macroporous monoliths with a specific surface area of 240 m^2/g or more with a single point total pore volume of around 0.4 cm^3/g.

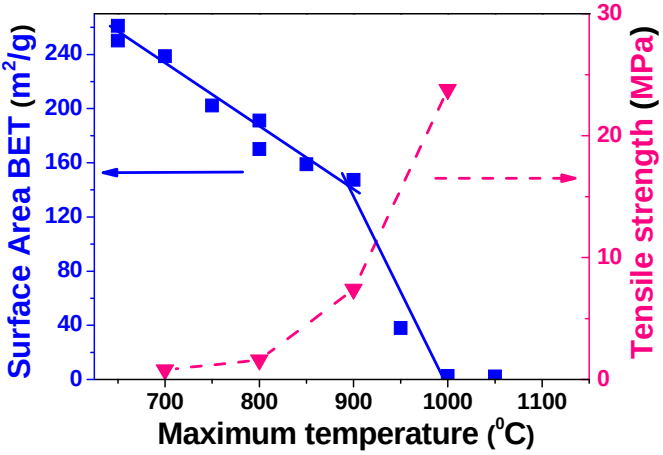

Figure 10. Correlation between the tensile strength and specific surface area of cylindrical monoliths produced from polydisperse mesoporous particles. The lines are guides for the eye.

The monolith's mechanical stability was evaluated using the diametral compression test on cylindrical monoliths prepared at different temperatures, as described in the experimental section. Figure 10 shows that the tensile strength

of the meso/macro porous silica monoliths depends strongly on the preparation temperature. Pulsed current processing of the mesoporous particles, at a T_{PCP} of 700°C, results in a monolith with a tensile strength of 0.8 MPa. Increasing the T_{PCP} to 800°C increases the strength to 1.6 MPa with only a slight decrease of the available surface area. Increasing the T_{PCP} to 900°C increases the strength substantially, reaching 7.4 MPa.

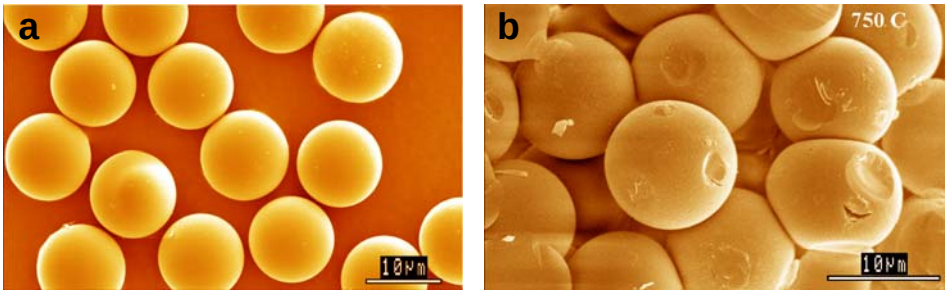

Figure 11. SEM micrographs of monodisperse mesoporous particles; (a) before and (b) after PCP processing at T_{PCP} of 750°C.

The size of the macropores can be tailored by the size and packing of the initial mesoporous powder. Figure 11a shows a SEM micrograph of monodisperse mesoporous particles prepared via an aerosol-assisted process using a vibrating orifice (see Experimental). The monodisperse particles have an average particle size of 12 µm and display a hexagonal mesostructure with an average pore size around 24 Å (not shown here). The assembly of the C_{16}TAB-templated mesoporous particles responds in a similar manner as the P123-templated particles to pulsed current processing. The larger monodisperse particles deform at the contact points and form a mechanically stable meso/macroporous monolith at T_{PCP} of 750°C (Figure 11b). The BET surface area of the monolith consisting of monodisperse mesoporous particles is 584 m^2g^{-1}, and mercury porosimetry data of the monolith shows a well-defined macropore size distribution between 1 and 4 µm, with a total macropore volume of 0.3 cm^3/g. Hence, increasing the average particle size about 10 times resulted in a hierarchically porous monolith where the size of the macropores also increased about 10 times.

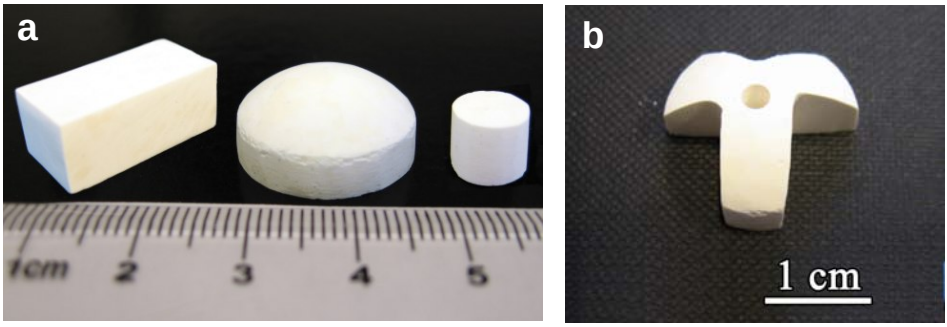

Figure 12. a) Meso/macroporous silica monoliths of different shapes prepared by rapid heating of an assembly of mesoporous particles in dies of different shapes (T_{PCP} of 700°C, 20 MPa); b) example of a shape that can be fabricated by machining of a meso/macroporous monolith. The original dome-shape monolith is depicted in the middle of Figure 12a.

PCP treatment of porous powders can also yield hierarchically porous monoliths of complex shape. The pulsed current processing of mesoporous particles yields monoliths that exactly replicate the shape of the fabrication die. Figure 12 gives examples of monoliths of cylindrical, dome-shaped and square shape. Problems with shrinkage and cracking that plague all solution-based methods are essentially absent. The monoliths have sufficient strength to allow well-established so-called green machining techniques, e.g. mechanical polishing, ultrasound milling and probably also laser cutting to be used.[144] Figure 12b gives an example of a simple shape that has been machined from the dome-shaped monolith.

4.1.2 Macro/macro porous monoliths

Macro/macro porous monoliths are important for different applications, e.g. filtration. High-purity diatomite powders with a silica content above 85% are currently used in waste water treatment and beverage filtration aids.[77, 145] The pulsed current processing technique has been used to consolidate diatomite powder into macro/macro porous mechanically stable monoliths.

The diatomite powders that have been used in this study have an SiO_2 content above 90%, which is considered to be a high-purity diatomite powder.[77] Other constituents are Al_2O_3, and Fe_2O_3 together with alkaline and alkaline earth oxides such as MgO, Na_2O, K_2O and smaller amounts of TiO_2 and P_2O_5. In fact, the composition of the diatomite powder in this study is comparable to the commercially available celite standard grade diatomite powder used for filter aids.[146]

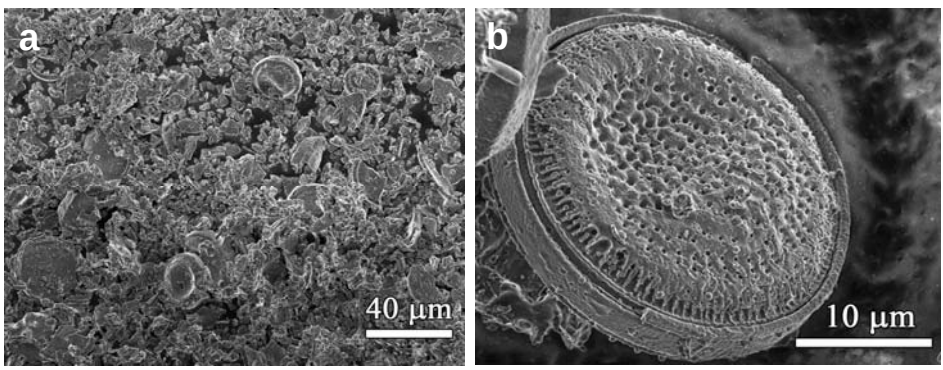

Figure 13. Scanning electron microscopy images of the as-received calcined diatomite powders at a) low magnification and b) higher magnification.

Figure 13a shows that the diatomite powder consists of plates, shells and broken particles. The unbroken diatomite particle in Figure 13b exhibits the intricate and highly porous structure typical of diatomite. Obviously, the mining of the diatomaceous earth and the post treatment results in a significant fraction of broken particles. The X-ray diffraction pattern in Figure 14a shows that the diatomite powder consists mainly of cristobalite. Hence, the heat treatment to PCP maximum temperature (T_{PCP}) of 900°C that the diatomite powder has been

subjected to is able to transform the originally amorphous silica into cristobalite without significant shape change. This shape-preserving crystallisation is of importance, because cristobalite has significantly larger chemical and thermal stability than amorphous silica.[131] The mercury intrusion data in Figure 14b displays two peaks: one strong peak with a pore size distribution around 2-4 µm, and one smaller peak around 0.2 µm. The pores around 2-4 µm are related to the voids between the powder particles, while the pores around 0.2 µm correspond to the inherent pore size of the diatomite powder (Figure 13b).

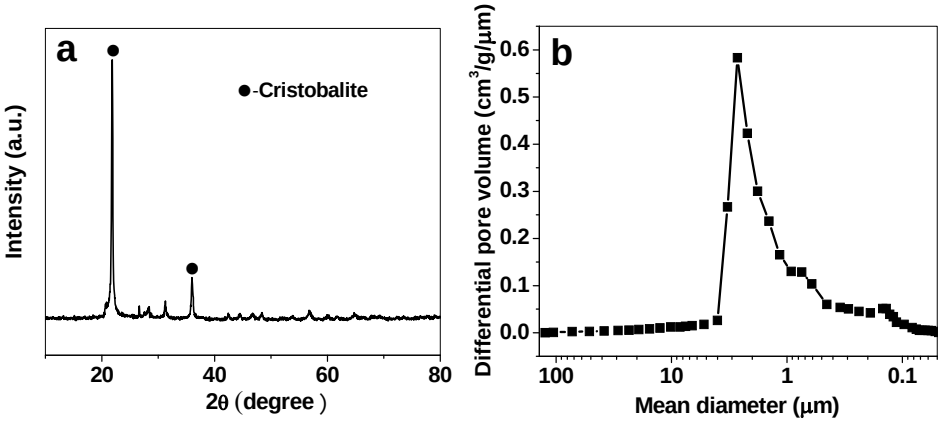

Figure 14. a) X-ray diffraction pattern of the as-received calcined diatomite powder. b) Mercury intrusion porosimetry of an assembly of the as-received calcined diatomite powder.

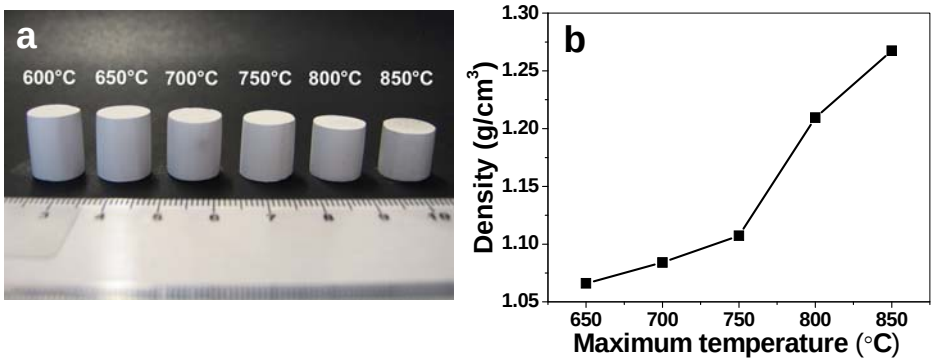

Figure 15. a) Cylindrical monoliths of diatomite powders that have been PCP-teated at various T_{PCP}. The change in height of the cylinders shows that the density increases with temperature. b) Bulk density as a function of T_{PCP}.

Figure 15a shows that crack free, cylindrical monoliths with a well defined volume can be produced using PCP over a range of T_{PCP}. The height and thus the volume of the monolithic cylinders decreases with increasing temperature, which shows that the density increases, since their weights were nearly identical. This is corroborated by the mercury porosimetry data (Table 2), which shows that the diatomite monoliths produced at 850°C have a porosity of 40 vol%. The change in density with T_{PCP} (Figure 15b) identifies three different temperature ranges for the densification process. At temperatures up to and including 650°C, the diatomite powder assembly does not shrink much. At this point, most of the interparticle pores in the powder body and the pores in the diatomite powder remain unaffected by the PCP treatment. Above 650°C, the density increases with temperature, and the densification process is enhanced at temperatures above 750°C. The diatomite powder collapses and forms a dense body at 1050°C (not shown).

Maximum temperature (T_{PCP}) (°C)	Pore volume[(a)] (cm^3/g)	Porosity (vol%)	Surface area[(b)] (m^2/g)	Median pore diameter[(c)] (µm)	Tensile strength[(d)] (MPa)
As-received	**N.A.**	**N.A.**	**2.4**	**2.69**	**N.A.**
650	**0.49**	**52**	**2.9**	**1.20**	**2.7**
750	**0.41**	**46**	**2.8**	**0.90**	**4.7**
850	**0.32**	**40**	**2.6**	**0.75**	**6.9**

Table 2. Pore volume, porosity, surface area, typical pore diameter and tensile strength of diatomite powder and diatomite monoliths consolidated at various temperatures.

[(a)] Total macropore volume calculated by mercury intrusion porosimetry.

[(b)] BET surface area calculated within 0.05 – 0.15 p/pº.

[(c)] Median pore diameter was estimated from mercury intrusion porosimetry data.

[(d)] Tensile strength obtained from diametral compression of cylindrical pellets.

The electron microscope images in Figure 16 show the microstructure of the diatomite powder assemblies at different temperatures. Figure 16a shows that the diatomite powders subjected to a T_{PCP} of 650°C remains relatively unaffected. The surface of the PCP treated diatomite powders displays circular pores similar to the as-received powder. The larger voids in the monolith relate to the pores between the diatomite powders. Increasing the T_{PCP} to 750°C (Figure 16b) leaves the diatomite powders relatively unaffected. A small fraction of the diatomite powder starts to melt, and the liquid phase accumulates in regions with negative curvature, i.e. at the contact points between two particles, to form necks. Increasing the T_{PCP} to 850°C (Figure 16c) results in more pronounced melting of the diatomite powder and a substantial collapse and closure of the internal porous structure.

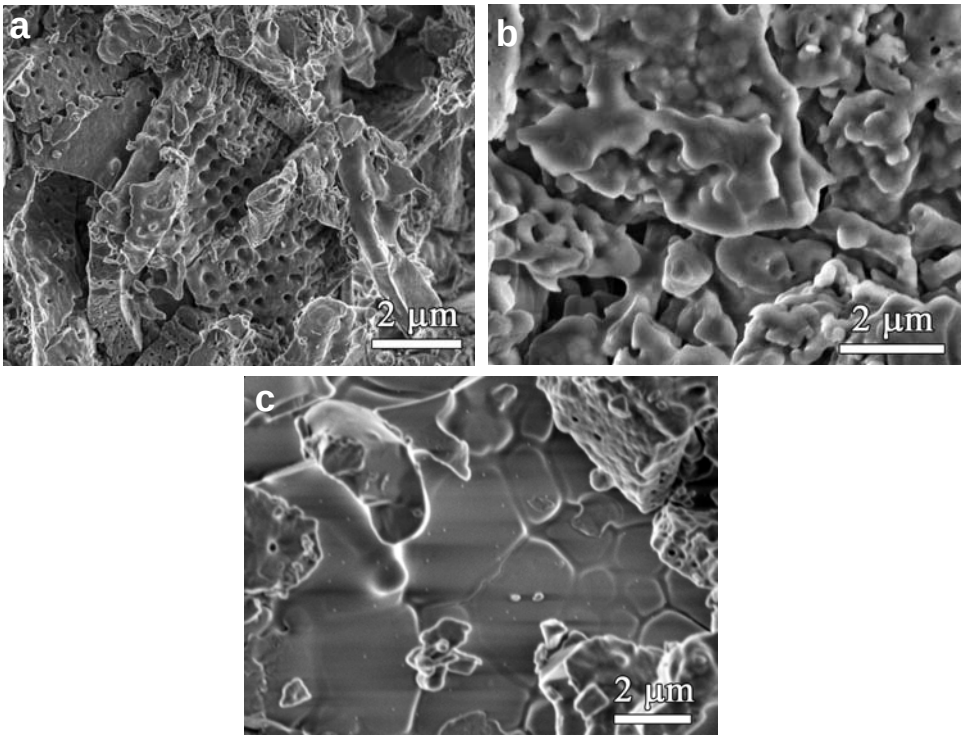

Figure 16. Scanning electron microscopy images of fractured surfaces of diatomite powder bodies that were processed at T_{PCP} of: a) 650°C, b) 750°C, c) 850°C.

The mercury intrusion data shows that the main peak shifts towards smaller pore size with increasing T_{PCP} (Table 2). Hence the size of the interparticle pores decreases as the T_{PCP} increases, and the interparticle voids become partially filled with the melt and/or collapse. It is possible to observe a small peak in the mercury intrusion curve around 0.2 μm, which relates to the intrinsic porosity of the diatomite powder for the monolith that was consolidated at T_{PCP} of 650°C.

We have also evaluated the mechanical stability of the porous diatomite monoliths, using the diametral compression test on cylindrical monoliths. Table 2 shows that the tensile strength of the diatomite monoliths depends strongly on the T_{PCP} (or porosity). Increasing the T_{PCP} to 750°C increases the strength to 4.7 MPa, with only a slight decrease in the porosity (46 vol.%). Increasing the T_{PCP} to 850°C increases the strength substantially, reaching 6.9 MPa, while the porosity decreases to 40 vol%.

4.1.3 Micro/macro porous monoliths

The pulsed current processing (PCP) technique was used to produce mechanically stable monoliths of different types of crystalline zeolite powders: ZSM-5 (with SiO_2/Al_2O_3 molar ratios of 280), zeolite Y (with SiO_2/Al_2O_3 molar ratios of 60 and 30) and silicalite-1. The crystal structures and pore connectivity of the zeolites are described in section 1.3.

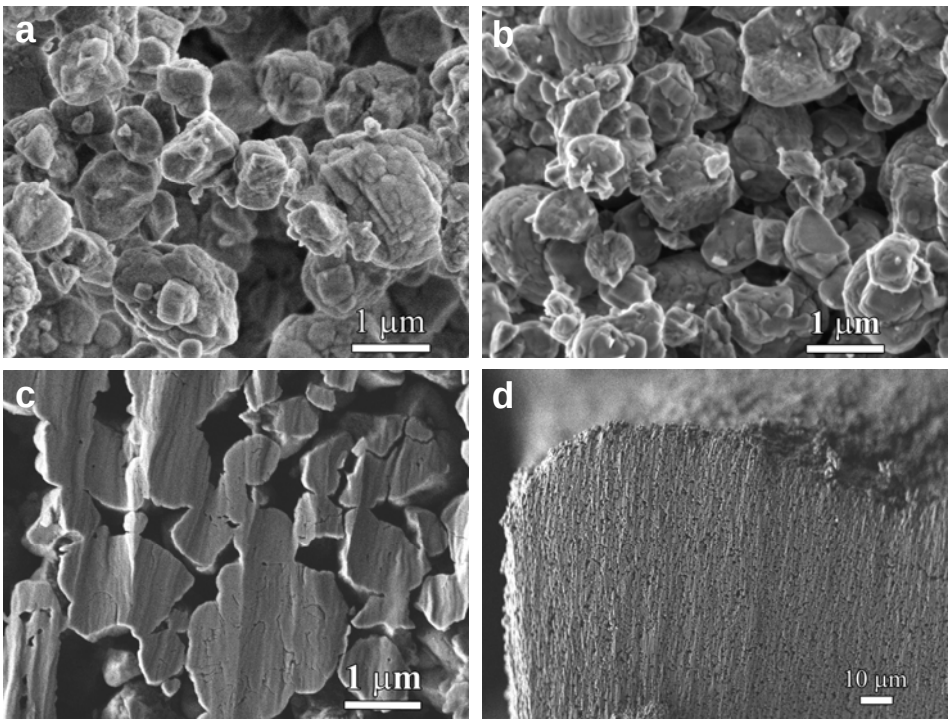

Figure 17**.** Scanning electron microscopy images: a) as-received ZSM-5 (280) powder; b) fractured and c) cross section polished surface of a monolith prepared at T_{PCP} of 1200°C; d) overview of the polished section of the monolith.

The ZSM-5 (280) powder is irregular and highly polydisperse, as shown in Figure 17a. The SEM image in Figure 17b does not reveal any structural or morphological changes in the zeolite powders in a monolith produced at 1200°C. This suggests that the heating and pressing affect only the connecting (touching) parts of the zeolite particles. The cross polished section of the same

sample prepared at PCP maximum temperature (T_{PCP}) of 1200°C, (Figure 17c) shows that the particles are connected.[147]

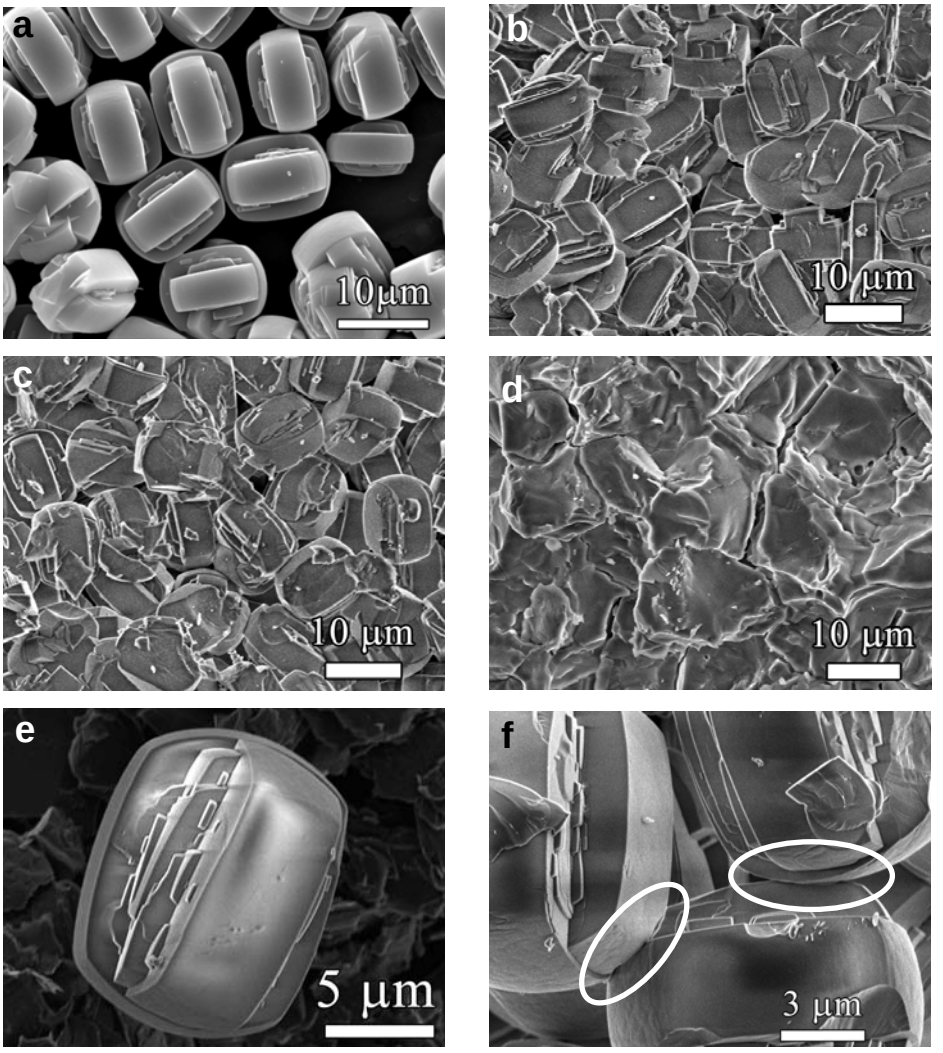

Figure 18**.** Scanning electron microscopy images of: a) as-received silicalite-1 powder; and fractured surfaces of silicalite-1 monolith prepared at T_{PCP} of b) 1000°C, c) 1100°C, d) 1300°C, e) magnified micrograph of single particle and f) particles processed at T_{PCP} of 1100°C and 20 MPa.

The as-prepared silicalite-1 particles have a narrow particle size distribution with an average size around 10×10×14 µm and a well-defined, faceted morphology (Figure 18a). Figure 1b shows that it is possible to treat the silicalite-1 particles by the pulsed current processing technique at a compressive pressure of 20 MPa and a T_{PCP} of 1100°C so as to form a powder body where the faceted morphology of the individual primary silicalite-1 particles is preserved. Increasing the T_{PCP} to 1300°C results in a collapse of the material and a significant loss of the characteristic features of the primary silicalite-1 particles (Figure 18c). This is corroborated by X-ray powder diffraction studies, which showed that PCP-treatment at T_{PCP} of 1200°C and above results in a significant loss of crystallinity and a subsequent transformation to α-cristobalite. The high-magnification scanning electron microscopy image in Figure 18d shows that the faceted silicalite-1 primary particles, PCP-treated at 20 MPa and 1100°C, have deformed or even collapsed locally at the contact points (shown by the white ovals). It is important to note the absence of any necks, i.e. material that has been transported to the grain boundaries, which suggests that sintering is insignificant under these conditions.

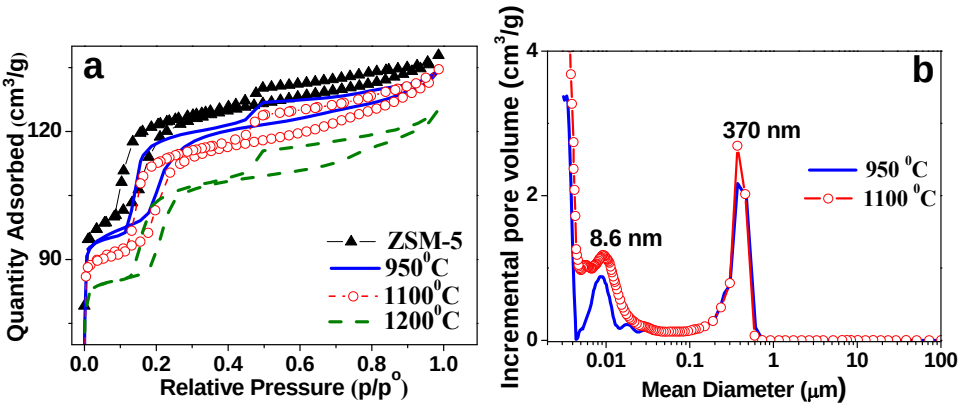

Figure 19. Characterization of porosity of as-received ZSM-5 zeolite powder and PCP-treated monoliths by a) nitrogen adsorption isotherms and b) mercury intrusion porosimetry.

The nitrogen sorption isotherms and the mercury intrusion pore size distribution data in Figure 19a and b show that the ZSM-5 (280) monoliths have a hierarchical pore structure, with micropores relating to the internal structure of

zeolite particles: mesopores (5-15 nm) and macropores (0.2-0.7 μm) that are a result of the interstices between the zeolite particles. The mercury intrusion data in Figure 19b confirms that the macroporosity does not change up to a T_{PCP} of 1200°C. The monolith preserves the high total pore volume (88% of as-received zeolite powder, calculated from the N_2-isotherm) and high surface area (79% of as-received zeolite powder, calculated from the N_2-isotherm) with a high mechanical stability of 2.4 MPa, see Table 3. At T_{PCP} of 1300°C the ZSM-5 zeolite structure collapsed and formed a glassy material.

The nitrogen sorption isotherms for silicalite-1 monoliths (Figure 20a) are typical for microporous materials. The silicalite-1 sample prepared at 1000°C shows a surface area of 97% of the original area for the as-received powder; the monolith PCP-treated at 1100°C has a surface area of 92% of the original value, see Table 2. At 1200°C, the surface area falls sharply to a very low value, which can be attributed to a collapse of the silicalite-1 microporous structure. The total pore volume of silicalite-1 monoliths also decreases gradually with PCP temperature, from 0.185cm^3/g (calcined silicalite-1 powder) and drops sharply to 0.031cm^3/g at 1200°C. Figure 20b shows that the macroporosity has a relatively narrow size distribution, which can be attributed to the uniform size of the synthesized silicalite-1 particles. The macropore volume of the silicalite-1 monoliths decreases gradually from 43vol% to 30vol% with increasing T_{PCP}.

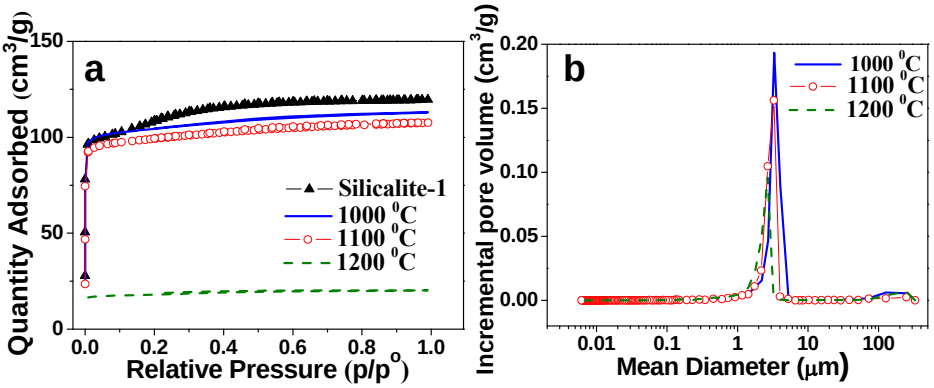

Figure 20. Characterization of the porosity of the as-received powder and monoliths PCP-treated at different T_{PCP} by a) nitrogen adsorption isotherms, and b) mercury intrusion porosimetry.

The change in the amorphous content with T_{PCP} and the induced lattice strain were estimated from an analysis of the PXRD data. Figure 21 shows how the strain and the amount of amorphous phase for ZSM-5 (280) vary with the maximum PCP temperature. The amorphous content increases linearly with the T_{PCP} in the temperature interval 950-1150°C, from 9% up to 35%. Above 1300°C, the ZSM-5 (280) completely transformes to an amorphous phase and no additional phase is formed. The grain size, as determined from the X-ray powder patterns, does not change up to 1150°C, being 170 nm for all samples, while the strain increases from 0.05% in the as-received material up to 0.17%, when the material has been subjected to a T_{PCP} of 1150°C.

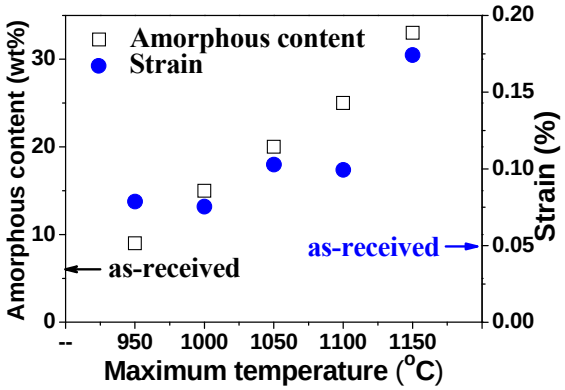

Figure 21. Calculated amorphous content and strain of ZSM-5 (280) monoliths as a function of T_{PCP}, determined using the Rietveld method.

We have performed a detailed study on how a different zeolite, zeolite Y, responds to PCP-treatment, by determining the strain, amount of amorphous phase and the unit cell parameter *a*. The as-received zeolite Y(30) and Y(60) powders have 43wt% and 36 wt% amorphous content, respectively. The origin of the high amorphous content is unclear, but as-synthesized zeolite can contain significant amounts of amorphous phase under certain synthesis conditions.[89, 90] The calculated amount of amorphous phase for zeolite Y monoliths shows almost no change up to T_{PCP} of 750°C (Figure 22a). Above 750°C, the amorphous content increases with increasing T_{PCP}. The increase commences at lower temperatures for zeolite Y(30), for which an increase of 60% of the normalised amorphous content occurs at a 50°C lower temperature than for zeolite Y(60). The normalized strain relative to 0.097% and 0.13% respectively

for the as-received zeolite Y(30) and Y(60), shows (Figure 22b) also a strong dependence on the T_{PCP}. The strain increases rapidly above 750°C for zeolite Y(30) and above 850°C for zeolite Y(60). The increase in strain probably reflects the increasing degree by which the PCP processing causes a deformation of the structure.

The normalized unit cell parameter *a* (a_0 = 24.2693(6) and a_0 = 24.2999(7) for zeolite Y(30) and Y(60), respectively) of zeolite Y is shown in Figure 22c. The PCP processing of zeolite Y powders induces a uniform contraction of the cubic unit, as shown in Figure 22c. The unit cell parameters of the PCP-treated zeolite Y(30) and Y(60) are very similar in the T_{PCP} range of 700-800°C. The observed decrease in unit cell volume with increasing T_{PCP} is probably related to the building up of strain in the PCP processed zeolite powders, Figure 22b.

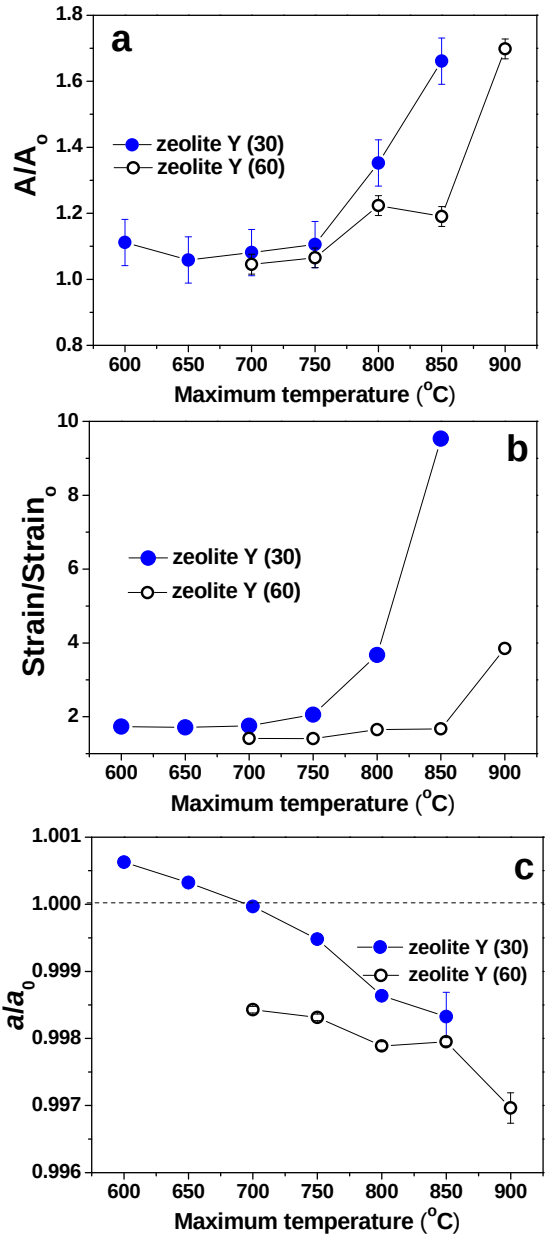

Figure 22. Normalized a) amorphous content (A/A_0), b) strain ($Strain/Strain_0$) and c) unit cell parameter a (a/a_0) as a function of T_{PCP} for zeolite Y(30) and Y(60).

Maximum temperature (T_{PCP}) (ºC)	Surface area[(a)] (m^2/g)	Total pore volume[(b)] (cm^3/g)	Total macropore volume[(c)] (cm^3/g)	Tensile strength[(d)] (MPa)
ZSM-5	**385**	**0.213**	**-**	**-**
950	**351**	**0.208**	**0.47**	**0.66**
1100	**333**	**0.203**	**0.44**	**1.6**
1200	**304**	**0.188**	**-**	**2.4**
1300	**2.47**	**0.0045**	**-**	**-**
Silicalite-1	**376**	**0.185**	**-**	**-**
1000	**363**	**0.174**	**0.39**	**-**
1100	**345**	**0.166**	**0.32**	**-**
1200	**62**	**0.031**	**0.22**	**-**

Table 3. Porosity and tensile strength of hierarchically porous pellets produced by PCP of ZSM-5 zeolite powder at different T_{PCP}, at an applied pressure of 20 MPa and a holding time of 3 minutes.

[(a)] BET surface area calculated within 0.05 – 0.15 p/pº.

[(b)] Single point adsorption total pore volume at relative pressure p/pº = 0.99 for pores < 142 nm.

[(c)] Total macropore volume calculated by mercury intrusion porosimetry.

[(d)] Tensile Strength obtained from diametral compression of cylindrical pellets.

Zeolite pellets for catalyst/adsorbent applications are exposed to mechanical stresses during transportation or storage and in the reactors. Therefore high mechanical strength is an important requirement for an industrial reactor.[148] We have evaluated the mechanical stability of the ZSM-5 pellets, using the diametral compression test on cylindrical pellets prepared at different temperatures. The data in Table 3 shows that the tensile strength of the zeolite monoliths depends strongly on the T_{PCP}. Increasing the T_{PCP} to 1100°C increases the strength to 1.6 MPa with only a slight decrease of the specific surface area. Increasing the T_{PCP} to 1200°C increases the strength substantially, reaching 2.4 MPa, while the specific surface area remains high. The strength is higher than that of zeolite pellets prepared with different binders[102] and substantially

higher than the strength of monoliths prepared by other solution-based binder-free techniques[108].

Xylene isomerisation was used as a probe reaction to evaluate the catalytic activity of the ZSM-5 material. Figure 23 shows that the product ratio for the PCP-treated material is only slightly lower than for the as-received ZSM-5 powder at the same conversion. The lower m-xylene/o-xylene ratio indicates that the mass transfer resistance of the crushed PCP-treated particles is higher than that of the as-received ZSM-5 powder, which can be related to the difference in aggregate size.

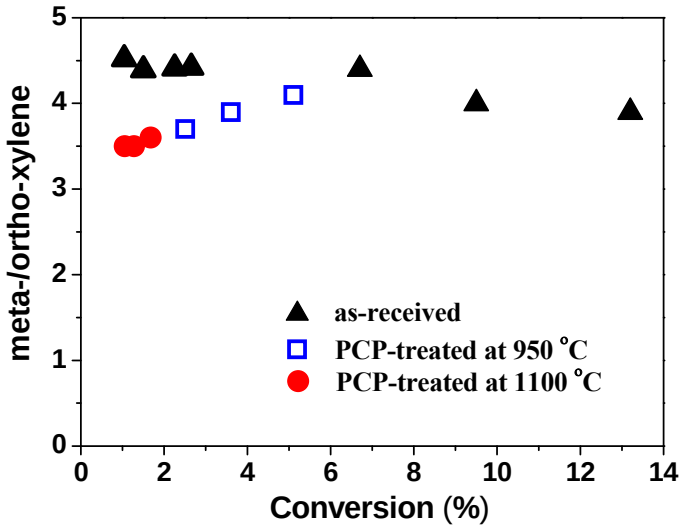

Figure 23. Product distribution (molar ratio of meta-/ortho-xylene) as a function of p-xylene conversion for the as-received ZSM-5 powder and the PCP-treated powder at a T_{PCP} of 950°C and 1100°C. The conversion was varied by varying the feed flow rate and the mass of catalyst in the reactor. For a catalyst mass of 1 g and 0.2 g, the observed p-xylene conversion varied between about 7-13%, and 1-3%, respectively, for the as received ZSM-5 powder.

4.2 Functionalization of mesoporous particles with TiO_2 nanoparticles

Previous work has shown that the aerosol-assisted route can generate spherical mesostructured powders from both aqueous and ethanol-based precursor solutions.[21, 23, 59] Here we show that direct functionalization of mesoporous particles is possible in an aerosol-assisted process. We studied how the direct addition of titania nanoparticles into the precursor solution influences the formation of mesoporous particles in the aerosol-assisted process. This is a novel route for the production of functionalized mesoporous particles for different applications, e.g. optical and catalytic.

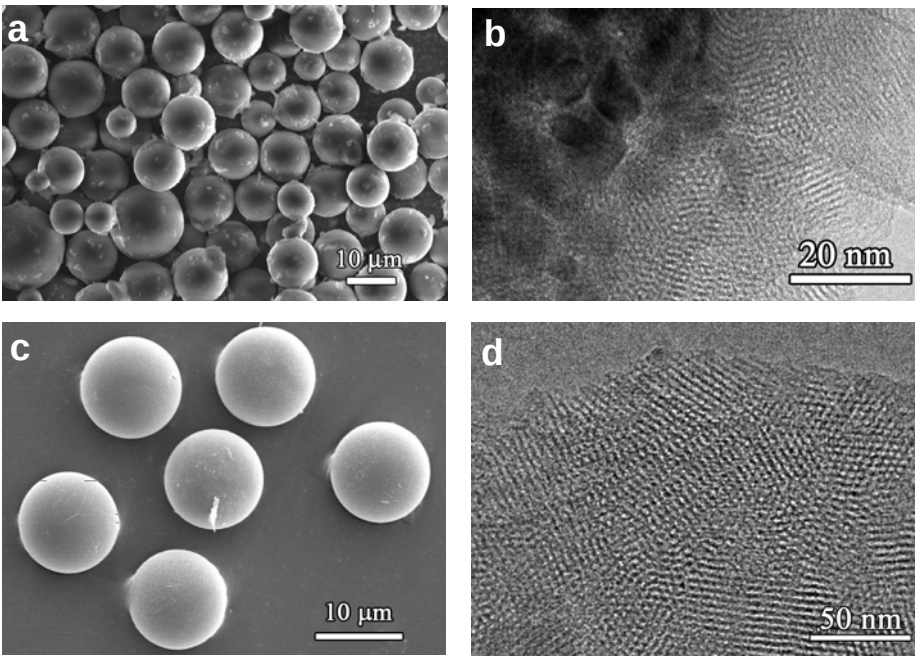

Figure 24. Templated spherical mesoporous silica particles produced from an aqueous-based precursor solutions: with TiO_2 nanoparticles a) SEM micrograph, b) TEM micrograph; and without addition of titania nanoparticles c) SEM micrograph and d) TEM micrograph.

By dispersing nanoparticles directly in the precursor solution it is possible to synthesize a composite powder where the titania nanoparticles are distributed inside the mesostructured matrix. Figure 24 shows electron microscopy micrographs of spherical mesoporous silica powders with and without TiO_2 nanoparticles. The polydispersity of mesoporous particles in Figure 24a is an effect of the titania addition, as can be seen when comparing with mesoporous particles that have been prepared from a precursor solution that does not contain any nanoparticles (Figure 24c).[59]

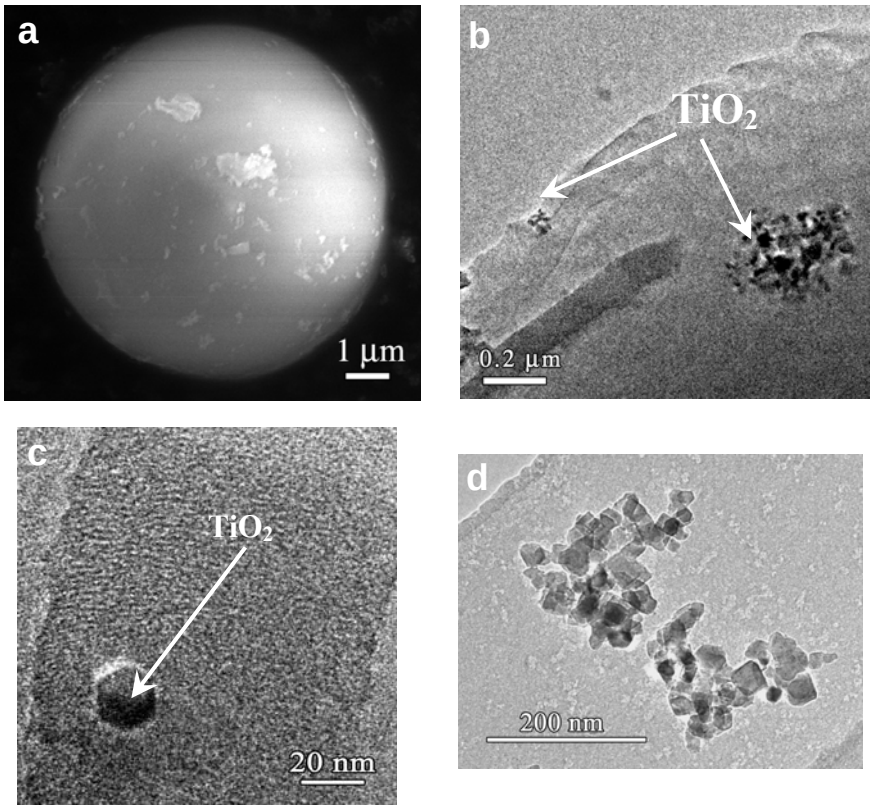

Figure 25. Electron micrographs of mesoporous particles functionalized with TiO_2 nanoparticles, from an ethanol-based solution: a) SEM micrograph of a single particle; b) and c) TEM micrographs of microtomed slices. d) TEM micrograph of crystallites of the as-received titania powder (P25, Degussa)

It is possible to identify the TiO_2 nanoparticles in the mesoporous matrix in the TEM images of crushed composite powders (Figure 24b). The dark clusters

are TiO_2 nanoparticles, which was also confirmed by TEM-EDX (not shown). A comparison of the mesostructure within the titania-containing powders with the mesostructure of powders produced without addition of titania nanoparticles (Figure 24d) indicates that the structure of the surfactant-templated mesopores is not significantly affected by the addition of the nanoparticles.

The problems of obtaining spherical shape and higher yield of powders when using aqueous solutions prompted us to produce nanoparticle-containing powders from ethanol-based dispersions. Figure 25a shows that the particles are spherical. The matrix surrounding the titania nanoparticles (Figure 25b) displays a mesostructure that appears to have a low degree of long-range order, characterized by domains with relatively disordered structure.

We have also sliced the mesoporous spheres containing titania nanoparticles, which were embedded in an epoxy resin, into thin sections by a microtome device. Microtomed slices of the mesoporous particles in Figure 25b clearly show that the TiO_2 nanoparticles have been successfully incorporated in the mesostructured matrix. Both single TiO_2 nanocrystals, with a size of approximately 28 nm (Figure 25c), and agglomerates of sizes between 70 nm and 300 nm (Figure 25b) can be found inside the mesostructured matrix. The TEM micrograph in Figure 25d shows that the powder consists of small crystallites with a size between 16 and 46 nm. The crystallite size corresponds reasonably well to an equivalent particle radius of 14 nm that can be estimated from the BET surface area of 50 m^2/g. The powder is agglomerated, and it was found that despite intense treatment with an ultrasonic horn it was not possible to reduce the agglomerate size below 190 nm. Hence, it appears that the size of the titania nanoparticles in the mesoporous matrix reflects the size of the primary agglomerates in the initial dispersion.[149]

The high-angle XRD pattern (Figure 26) confirms the presence of TiO_2 nanoparticles within the mesoporous silica particles. It is clear that the aerosol-assisted synthesis and subsequent calcination did not affect the crystal structure of the TiO_2 nanoparticles. The positions of the main peaks observed in the XRD patterns of particles correspond to the mixture of anatase and rutile phases of TiO_2 that was found in the as-received powder (3.7:1).

Measurements of the specific surface area and total pore volume of the spherical mesoporous particles, calculated from the N_2-adsorption/desorption isotherms, showed that incorporation of 1.9wt% of TiO_2 nanoparticles causes a slight reduction of the specific surface area and total pore volume from 950

m^2/g and 0.5 cm^3/g to 806 m^2/g and 0.364 cm^3/g, without and with addition of nanoparticles respectively.

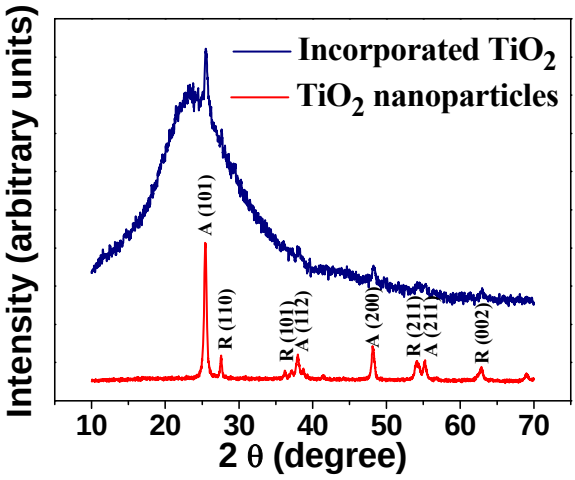

Figure 26. High-angle x-ray diffraction patterns of as-received TiO_2 nanoparticles (P25 Degussa), and mesoporous silica particles functionalized with TiO_2 nanoparticles from ethanol-based solution.

Increasing the concentration of TiO_2 nanoparticles 10 times (from 1.9wt% to 19wt%) results in mesoporous powders with a particle size distribution similar to that of the powder with 1.9wt% of TiO_2 nanoparticles. The yield is substantially reduced, which could be related to partial clogging of the orifice. Hence, it is clear that the introduction of nanoparticles into the precursor solution can induce instabilities in the liquid jet at the vibrating orifice.

5 Conclusions

Novel methods to functionalize mesoporous materials and produce hierarchically porous materials have been developed.

1. Mechanically stable, hierarchically porous silica monoliths were fabricated by the pulsed current processing technique, using different porous powders. Rapid heating of powder assemblies subjected to a compressive stress results in a small deformation of the porous particles at the contact points which gives mechanical stability to the porous monoliths, while the initial porous structure is preserved. This technique yields macroscopic bodies that exactly replicate the shape of the fabrication die, and which can be further machined to yield complex shapes. The total process time from loading the die with the powder to removing the shaped porous body is less than 30 minutes, and the size of the object is basically limited by the die size.

Mechanically stable meso/macroporous silica monoliths, with tunable open macropores and template-controllable ordered mesopores, were fabricated using monodisperse and polydisperse aerosol-generated spherical mesoporous particles. Restricting the T_{PCP} to 750°C results in monoliths with bimodal porosity and high mechanical stability, where the mesopores are virtually unaffected by the heating process.

Macro/macroporous ceramic monoliths were fabricated from a cheap and renewable natural resource: diatomite powder. The results showed that consolidation of calcined diatomite particles proceeds by the formation of necks at temperatures around 700-750°C which is followed by significant melt phase formation when the temperature is increased to 850°C. The diatomite monoliths with high porosity can find applications in beverage purification and waste water treatment.

Mechanically stable, micro/macroporous porous monoliths were fabricated by PCP using different crystalline microporous powders: ZSM-5, zeolite Y and silicalite-1. Rietveld refinement based on X-ray diffraction data and scanning electron microscopy showed that the formation of strong interparticle bonds during the PCP process is associated with an amorphization reaction. The ZSM-5 micro/macroporous monoliths retained a high catalytic selectivity as illustrated by xylene isomerisation. The possibility of producing strong, binder-

free, hierarchically porous micro/macroporous monoliths of arbitrary shape opens up new adsorbent and catalytic applications where the mechanochemical conditions are very demanding.

2. Direct (in-situ) functionalization of surfactant templated mesoporous silica spheres with pre-synthesized TiO_2 nanoparticles was demonstrated by the use of an aerosol-assisted process. The addition of the nanoparticles results in a small reduction of the specific surface area and total pore volume of the mesoporous sphere. The use of an ethanol-based system results in better particle yield, while the mesostructure has a more defined long-range order when the spheres have been produced from an aqueous system. The aerosol-assisted technique can be used to introduce various types of nanoparticles, and it thus offers a viable route for the production of multifunctional colloids that are of interest for various applications, e.g. in water treatment, catalysis and chromatography.

6 Future work

There are many things to understand and to discover in this new field of preparation of hierarchically porous monoliths by the pulsed current processing technique. We are at the beginning of an interesting study. Careful and thorough analysis is necessary to understand different processes and phenomena involved in the formation of shaped bodies by PCP, where porous monoliths must combine different properties e.g. high mechanical stability, high porosity and adsorbent or catalytic properties in order to achieve a required product.

First, zeolites with different structures should be pulsed current processed at different heating rates (e.g. 100°C/min, 200°C/min) and higher pressures (e.g. 40 MPa and 100 MPa), in order to yield an understanding of the processing behaviour. Second, the mechanism of amorphization must be studied in detail. The progress of amorphization e.g. development of possible pore collapse and amorphous content gradient inside the pellet depending on temperature, pressure and holding time should be carefully studied by HRTEM and HRSEM on ion-beam sliced processed zeolites. Amorphization may also be studied by e.g. ^{129}Xe Nuclear Magnetic Resonance (NMR) to quantify the amount of amorphous phase and the presence of intergrowths and of non-framework species. XRD data should be also investigated by Vonk method, where evaluation of background profile can be used to quantify of amorphous content. Migration of Al sites during the PCP is possible and can be studied by ^{29}Si magic angle spinning (MAS) NMR spectroscopy to calculate framework Si/Al ratio. Fourier transform Infrared (FTIR) and NMR spectroscopies can be used to evaluate the acidity of the processed zeolites. Third, different properties of the processed pellets should be investigated, e.g. catalytic and adsorbent. Finally, other porous materials should be tried e.g. carbon-based materials and mixture of different zeolites to form functionally graded materials.

Direct functionalization of the mesoporous particles in the aerosol-assisted process and in sol-gel process can be tried with nanoparticles e.g. TiO_2, Fe_3O_4 and CeO_2. Such systems should be studied for bio, catalytic and separation applications. The nanoparticle functionalized mesoporous particles should be also processed by PCP technique to produce hierarchically porous bodies which advanced e.g. catalytic properties. Also post-functionalization of the

hierarchically porous monoliths with organic molecules should be tried and tested for different applications, e.g. CO_2 separation.

7 Acknowledgments

First of all I would like to thank my excellent supervisor *Prof. Lennart Bergström* for constant support, encouragement and fantastic ideas.

This work would not have been possible to do without the continual support of following people:

I wish to express my sincere gratitude to *Prof. Zhijian Shen (James), Assoc. Prof. Jekabs Grins, Doc. Niklas Hedin, Dr. Yasuhiro Sakamoto, Dr. Robert Hodgkins, Dr. Kjell Jansson, Dr. Ainiwaer Aheniyazi Assoc. Prof. Johnsson, Mats* and *Boon Sing Ng (Jovice)* for their significant assistance and invaluable advice throughout this work.

I would like to thank *Dr. Peter Alberius* and *Dr. Nina Anderson* at YKI for valuable discussions and for the synthesis of the polydisperse mesoporous particles.

I would like to thank *Pelle Jansson* for help with set-up and development of the aerosol reactor.

I would like to thank *Prof. Mats Nygren* and *Dr. David Salamon* for valuable discussions and assistance with the SPS experiments.

I would like to acknowledge guidance and discussion on XRD measurements with *Assoc. Prof. Jekabs Grins*, *Assoc. Prof. Lars Eriksson* at SU *and Dr. Andreas Fischer* at KTH .

I would like to thank *Assist. Prof. Alfonso Garcia-Bennett* for introduction of mesoporous materials, guidance and discussions on TEM measurements.

I would like to thank *Bertrand Faure* for his assistance with the nanoparticle functionalization work and *Arto Ojuva* for his assistance with the zeolite amorphization by PCP.

I would like to thank *Prof. Jonas Hedlund*, *Assist. Prof. Johanne Mouzon*, and *Dr. Charlotte Andersson*, at the Division of Chemical Engineering, Luleå University of Technology for their help and discussions on catalytic measurements and for preparation of sililite-1 particles.

I would like to thank *Prof. Derek Creaser*, *Dr. Indra Perdana* and *Dr. Kompiang Wirawan* for support and discussions on NH_3 TPD measurements at the Department of Chemical and Biological Engineering, Chalmers University.

I would like to thank *Dr. Sigita Urbonaite* and *Dr. Kristina Lund* for their help with and advice on the N_2 sorption measurement.

I wish to thank *Dr. Keiichi Miyasaka* and *Dr. Peter Oleynikov* for discussions and for help with preparation of visualization of materials.

I wish to acknowledge the professional help of *Ann-Britt Rönnell* and *Eva Peterson* and the very efficient help with literature of *Hillevi Isaksson* .

I wish to express my gratitude to *Prof. Osamu Terasaki*, *Prof. Xiaodong Zou*, *Prof. Sven Hovmöller, Prof. Sven Lidin* and *Prof. Margareta Sundberg* for their interesting lectures/seminars and for invaluable advice and discussions.

I would like to acknowledge the help and professionalism of SU Innovation – *Dr. Mona Wilcke* and *Ulf Erickson*, SU Holding – *Dr. Thomas Arctaedius* and to thank all the people at the SU Innovation office for very nice atmosphere and discussions.

I would like to acknowledge *Assos. Prof. Saeid Esmaeilzadeh* and *Assos. Prof. Armando Córdova* for valuable discussions.

I am grateful to all members of the Materials Chemistry group for a good time, for fantastic parties and an encouraging working atmosphere:

Dr. German Salazar-Alvarez, Baroz Aziz, Linnea Andersson, Erik Wetterskof, Dr. Sato Kimiyasu, Dr. Bacsik Zoltan, Jovice Boonsing Ng, Dr. Weber Jens, Dr. Denis Gebauer, Dr. Oliynyk Vitaliy, Dr. Subhasis Rana, Dr. Satoshi Tanaka, Dr. Ainiwaer Aheniyazi, *Dr. Robert Hodgkins*

and other people at the Physical, Inorganic and Structural Chemistry Department,

especially *Dr. Leonova Ekaterina, Ehsan Jalilian, Mirva Eriksson, Dr. Jegou Simon, Iftekhar Shahriar, Dr. Ali Sharafat, Alexander Mirzoev, Evgeny Polyakov, Dr. Nikolai Volkov, Zoltan Takacs, David Moser, Sam Stevens, Mikaela Gustafsson and Miia Klingstedt.*

I wish to acknowledge the funding this project by the Swedish Science Council (VR), Berzelii centre Exselent on porous materials, Swedish Institute for FA and the Wallenberg foundation.

I would like to acknowledge my previous supervisors and teachers:
Prof. Zhores Ivanovich Alferov, Prof. Semen Grigor'evich Konnikov, *Prof. Alexandr Yakovlevich Vul,* and *Prof. Vladimir Il'ich Korol'kov* at Ioffe Physical Technical Institute,
Prof. Georgiy Nikolaevich Fursey at University of Telecommunications,

Prof. Toshiaki Enoki and *Prof. Ken-Ichi Fukui* at Tokyo Institute of Technology.

I would like to express my gratitude to my friends in Russia:

Dr. Lev L. Kuandykov, Sergey A. Fomin and *Nikolaeva Maria, Anton Kotov, Pavel Tret'yakov, Anastasiya Ganatovskaya, Anastasiya Zlatopol'skaya, Natalia Shveyeva, Irina Sergeeva* and *Dr. Max Sokolov*,

and around the world:

Fernando Rodriges, Ruben, Alberto Marini, Dr.Andrey Novoselov, Dr.Konstantin Nikitin and *Olga Nikitina, Dr.Osipov Vladimir, Anna Skochilenko, Otsubo Yusuke, Dr.Edward Whittaker, Benitez Erick, Garcia Leo, Tsushima Ayako, Antony Hartley, Richard Gabler, Dr.Denis Searby, Dr. Anders Jarfors, Prof. Tan Ser Peow, Guram Khandamishvili, Ekaterina Rozenkrants, Sergey Osmekhin, Anastassia Stolovitskaia, Dr. Vinicius Lobosco, Erwan Le Moigne*, *Pavel Demchenko and Karina Harexian.*

for valuable discussions, good times, feelings and understanding.

I would like to say thank you to my dear *Kseniya Kornilova* for your understanding, love and support.

Finally, I would like to express my gratitude to my mother *Tatyana V. Vasilieva*, my brother *Andrey O. Vasiliev* and my grandparents *Galina P. Yasyuchenya, Valentin A. Yasyuchenya. Raisa A. Vasilieva and Vladimir I. Vasiliev*, who have given all their love to support my career and to encourage me to be as I am.

8 References

1. Everett, D.H., *IUPAC, manual of symbols and terminology.* Pure and Applied Chemistry, 31(4): p. 579, 1972.
2. Yanagisawa, T., et al., *The preparation of alkyltrimethylammonium-kanemite complexes and their conversion to microporous materials.* Bulletin of the Chemical Society of Japan, 63(4): p. 988-992, 1990.
3. Beck, J.S., et al., *A new family of mesoporous molecular sieves prepared with liquid crystal templates.* J. Am. Chem. Soc., 114: p. 10834-10843, 1992.
4. Kresge, C.T., et al., *Ordered mesoporous molecular sieves synthesized by a liquid-crystal template mechamism.* Nature, 359: p. 710-712, 1992.
5. Kresge, C.T., et al., *Composition of synthetic porous crystalline material, its synthesis*, 5102643 470008, 1990.
6. Di Renzo, F., H. Cambon, and R. Dutartre, *A 28-year-old synthesis of micelle-templated mesoporous silica.* Microporous Materials, 10(4-6): p. 283-286, 1997.
7. Studart, A.R., et al., *Processing routes to macroporous ceramics: A review.* Journal of the American Ceramic Society, 89(6): p. 1771-1789, 2006.
8. Colombo, P., *Conventional and novel processing methods for cellular ceramics.* Philosophical Transactions of the Royal Society a-Mathematical Physical and Engineering Sciences, 364(1838): p. 109-124, 2006.
9. Stein, A. and R.C. Schroden, *Colloidal crystal templating of three-dimensionally ordered macroporous solids: materials for photonics and beyond.* Current Opinion in Solid State and Materials Science, 5(6): p. 553-564, 2001.
10. Barton, T.J., et al., *Tailored porous materials.* Chemistry of Materials, 11(10): p. 2633-2656, 1999.
11. Kitagawa, S., R. Kitaura, and S. Noro, *Functional porous coordination polymers.* Angewandte Chemie-International Edition, 43(18): p. 2334-2375, 2004.
12. Rowsell, J.L.C. and O.M. Yaghi, *Metal-organic frameworks: a new class of porous materials.* Microporous and Mesoporous Materials, 73(1-2): p. 3-14, 2004.
13. Zhao, D.Y., et al., *Triblock copolymer syntheses of mesoporous silica with periodic 50 to 300 angstrom pores.* Science, 279(5350): p. 548-552, 1998.
14. Hodgkins, R.P., A.E. Garcia-Bennett, and P.A. Wright, *Structure and morphology of propylthiol-functionalised mesoporous silicas templated*

by non-ionic triblock copolymers. Microporous and Mesoporous Materials, 79(1-3): p. 241-252, 2005.
15. Fan, J., et al., *Cubic mesoporous silica with large controllable entrance sizes and advanced adsorption properties.* Angewandte Chemie-International Edition, 42(27): p. 3146-3150, 2003.
16. Attard, G.S., J.C. Glyde, and C.G. Goltner, *Liquid-crystalline phases as templates for the synthesis of mesoporous silica.* Nature, 378(6555): p. 366-368, 1995.
17. Lu, Y.F., et al., *Continuous formation of supported cubic and hexagonal mesoporous films by sol gel dip-coating.* Nature, 389(6649): p. 364-368, 1997.
18. Klotz, M., et al., *Synthesis conditions for hexagonal mesoporous silica layers.* Journal of Materials Chemistry, 10(3): p. 663-669, 2000.
19. Honma, I., et al., *Structural control of surfactant-templated hexagonal, cubic, and lamellar mesoporous silicate thin films prepared by spin-casting.* Advanced Materials, 12(20): p. 1529-1533, 2000.
20. Zhao, D., et al., *Continuous mesoporous silica films with highly ordered large pore structures.* Advanced Materials, 10(16): p. 1380-+, 1998.
21. Bruinsma, P.J., et al., *Mesoporous silica synthesized by solvent evaporation: Spun fibers and spray-dried hollow spheres.* Chemistry of Materials, 9(11): p. 2507-2512, 1997.
22. Yang, P.D., et al., *Triblock-copolymer-directed syntheses of large-pore mesoporous silica fibers.* Chemistry of Materials, 10(8): p. 2033-+, 1998.
23. Lu, Y.F., et al., *Aerosol-assisted self-assembly of mesostructured spherical nanoparticles.* Nature, 398(6724): p. 223-226, 1999.
24. Grosso, D., et al., *Nanocrystalline transition-metal oxide spheres with controlled multi-scale porosity.* Advanced Functional Materials, 13(1): p. 37-42, 2003.
25. Huo, Q.S., et al., *Organization of organic-molecules with inorganic molecular-species into nanocomposite biphase arrays.* Chemistry of Materials, 6(8): p. 1176-1191, 1994.
26. Raman, N.K., M.T. Anderson, and C.J. Brinker, *Template-based approaches to the preparation of amorphous, nanoporous silicas.* Chemistry of Materials, 8(8): p. 1682-1701, 1996.
27. Andersson, N., *Aerosol based synthesis of functionalized mesostructured materials*. Licentiate Thesis. Stockholm: Stockholm University, 2005.
28. Chen, C.Y., et al., Microporous Materials, 2: p. 27, 1993.
29. Ogawa, M., *Formation of novel oriented transparent films of layered silica-surfactant nanocomposites.* Journal of the American Chemical Society, 116(17): p. 7941-7942, 1994.

30. Brinker, C.J., et al., *Evaporation-induced self-assembly: Nanostructures made easy.* Advanced Materials, 11(7): p. 579-+, 1999.
31. Ji, X.L., et al., *Synthesis and characterization of functionalized mesoporous silica by aerosol-assisted self-assembly.* Chemistry of Materials, 18(9): p. 2265-2274, 2006.
32. Alonso, B., et al., *New routes to mesoporous silica-based spheres with functionalised surfaces.* Chemical Communications, (13): p. 1746-1748, 2005.
33. Andersson, N., et al., *Photochromic mesostructured silica pigments dispersed in latex films.* Journal of Materials Chemistry, 15(34): p. 3507-3513, 2005.
34. Lu, Y.F., et al., *Evaporation-induced self-assembly of hybrid bridged silsesquioxane film and particulate mesophases with integral organic functionality.* Journal of the American Chemical Society, 122(22): p. 5258-5261, 2000.
35. Hampsey, J.E., et al., *One-step synthesis of mesoporous metal-SiO_2 particles by an aerosol-assisted self-assembly process.* Chemistry of Materials, 17(9): p. 2475-2480, 2005.
36. Lu, Y.F., et al., *Self-assembly of mesoscopically ordered chromatic polydiacetylene/silica nanocomposites.* Nature, 410(6831): p. 913-917, 2001.
37. Vinu, A., K.Z. Hossain, and K. Ariga, *Recent advances in functionalization of mesoporous silica.* Journal of Nanoscience and Nanotechnology, 5(3): p. 347-371, 2005.
38. Kim, J., et al., *Magnetic fluorescent delivery vehicle using uniform mesoporous silica spheres embedded with monodisperse magnetic and semiconductor nanocrystals.* Journal of the American Chemical Society, 128(3): p. 688-689, 2006.
39. Wu, P.G., J.H. Zhu, and Z.H. Xu, *Template-assisted synthesis of mesoporous magnetic nanocomposite particles.* Advanced Functional Materials, 14(4): p. 345-351, 2004.
40. Uchiyama, H., et al., *A novel adsorbent photocatalyst consisting of titania and mesoporous silica nanoparticles.* Materials Science and Engineering B-Solid State Materials for Advanced Technology, 123(3): p. 248-251, 2005.
41. Inumaru, K., et al., *Direct nanocomposite of crystalline TiO_2 particles and mesoporous silica as a molecular selective and highly active photocatalyst.* Chemical Communications, (16): p. 2131-2133, 2005.
42. Busuioc, A.M., et al., *Structural features and photocatalytic behaviour of titania deposited within the pores of SBA-15.* Applied Catalysis a-General, 312: p. 153-164, 2006.

43. He, X. and D. Antonelli, *Recent advances in synthesis and applications of transition metal containing mesoporous molecular sieves.* Angewandte Chemie-International Edition, 41(2): p. 214-229, 2001.
44. Bronstein, L.M., *Nanoparticles made in mesoporous solids*, in *Colloid Chemistry 1*. 55-89. Berlin: Springer-Verlag Berlin. 2003.
45. Mulukutla, R.S., et al., *Nanosized rhodium oxide particles in the MCM-41 mesoporous molecular sieve.* Chemical Communications, (14): p. 1425-1426, 1998.
46. Zhang, Z.T., et al., *Controlled synthesis of CdS nanoparticles inside ordered mesoporous silica using ion-exchange reaction.* Journal of Physical Chemistry B, 105(29): p. 6755-6758, 2001.
47. Zhang, L., G.C. Papaefthymiou, and J.Y. Ying, *Synthesis and properties of gamma-Fe_2O_3 nanoclusters within mesoporous aluminosilicate matrices.* Journal of Physical Chemistry B, 105(31): p. 7414-7423, 2001.
48. Dag, O., et al., *Photoluminescent silicon clusters in oriented hexagonal mesoporous silica film.* Advanced Materials, 11(6): p. 474-+, 1999.
49. Zelenak, V., et al., *Mesoporous silica modified with titania: Structure and thermal stability.* Chemistry of Materials, 18(14): p. 3184-3191, 2006.
50. Hirai, T., H. Okubo, and I. Komasawa, *Incorporation of CdS nanoparticles formed in reverse micelles into mesoporous silica.* Journal of Colloid and Interface Science, 235(2): p. 358-364, 2001.
51. Hodgkins, R.P., et al., *Maghemite nanocrystal impregnation by hydrophobic surface modification of mesoporous silica.* Langmuir, 23(17): p. 8838-8844, 2007.
52. Konya, Z., et al., *Synthetic insertion of gold nanoparticles into mesoporous silica.* Chemistry of Materials, 15(6): p. 1242-1248, 2003.
53. Adams, W.A., et al., *Synthesis and characterization of mesoporous silica films encapsulating titanium dioxide particles photodegradation of 2,4-dichlorophenol.* Journal of Hazardous Materials, 112(3): p. 253-259, 2004.
54. Bore, M.T., et al., *Synthesis of Pt nanowires inside aerosol derived spherical mesoporous silica particles.* Catalysis Letters, 98(4): p. 167-172, 2004.
55. Unger, K.K., et al., *Synthesis of spherical porous silicas in the micron and submicron size range: challenges and opportunities for miniaturized high-resolution chromatographic and electrokinetic separations.* Journal of Chromatography A, 892(1-2): p. 47-55, 2000.
56. Huo, Q.S., et al., *Preparation of hard mesoporous silica spheres.* Chemistry of Materials, 9(1): p. 14-&Accounts of Chemical Research Acc. Chem. Res., 1997.

57. Qi, L.M., et al., *Micrometer-sized mesoporous silica spheres grown under static conditions.* Chemistry of Materials, 10(6): p. 1623-1626, 1998.
58. Fowler, C.E., D. Khushalani, and S. Mann, *Interfacial synthesis of hollow microspheres of mesostructured silica.* Chemical Communications, (19): p. 2028-2029, 2001.
59. Rao, G.V.R., et al., *Monodisperse mesoporous silica microspheres formed by evaporation-induced self assembly of surfactant templates in aerosols.* Advanced Materials, 14(18): p. 1301-+, 2002.
60. Bore, M.T., et al., *Hexagonal mesostructure in powders produced by evaporation-induced self-assembly of aerosols from aqueous tetraethoxysilane solutions.* Langmuir, 19(2): p. 256-264, 2003.
61. Andersson, N., et al., *Structural features and adsorption behaviour of mesoporous silica particles formed from droplets generated in a spraying chamber.* Microporous and Mesoporous Materials, 72(1-3): p. 175-183, 2004.
62. B. Gates, Y.X., *Fabrication and characterization of chirped 3D photonic crystals.* Advanced Materials, 12(18): p. 1329-1332, 2000.
63. Fleischhaker, F., et al., *Photochemically and thermally tunable planar defects in colloidal photonic crystals.* Journal of the American Chemical Society, 127(26): p. 9318-9319, 2005.
64. Galassi, C., *Processing of porous ceramics: Piezoelectric materials.* Journal of the European Ceramic Society, 26(14): p. 2951-2958, 2006.
65. Greil, P., *Advanced engineering ceramics.* Advanced Materials, 14(10): p. 709-716, 2002.
66. Scheffler, M. and P. Colombo, *Cellular Ceramics: Structure, Manufacturing, Properties and Applications.* Weinheim: Wiley-VCH, 2005.
67. Green, D.J. and R. Colombo, *Cellular ceramics: Intriguing structures, novel properties, and innovative applications.* Mrs Bulletin, 28(4): p. 296-300, 2003.
68. Ueno, S., L.M. Lin, and H. Nakajima, *Formation mechanism of porous alumina with oriented cylindrical pores fabricated by unidirectional solidification.* Journal of the American Ceramic Society, 91(1): p. 223-226, 2008.
69. van Setten, B., et al., *Stability of catalytic foam diesel-soot filters based on Cs_2O, MoO_3, and Cs_2SO_4 molten-salt catalysts.* Applied Catalysis B-Environmental, 42(4): p. 337-347, 2003.
70. Dhar, G.M., et al., *Mixed oxide supported hydrodesulfurization catalysts - a review.* Catalysis Today, 86(1-4): p. 45-60, 2003.

71. Nair, J., et al., *Influence of peptization and ethanol washing on the pore-structure evolution of sol-gel-derived alumina catalyst supports.* Journal of the American Ceramic Society, 81(10): p. 2709-2712, 1998.
72. Falamaki, C., M. Naimi, and A. Aghaie, *Dual behavior of $CaCO_3$ as a porosifier and sintering aid in the manufacture of alumina membrane/catalyst supports.* Journal of the European Ceramic Society, 24(10-11): p. 3195-3201, 2004.
73. Li, S.H., et al., *Novel method to manufacture porous hydroxyapatite by dual-phase mixing.* Journal of the American Ceramic Society, 86(1): p. 65-72, 2003.
74. Kim, H.W., J.C. Knowles, and H.E. Kim, *Mechanical and biological performance of calcium phosphate coatings on porous bone scaffold.* Journal of the American Ceramic Society, 87(11): p. 2135-2138, 2004.
75. Zhao, J. and X.D. Yang, *Photocatalytic oxidation for indoor air purification: a literature review.* Building and Environment, 38(5): p. 645-654, 2003.
76. Gogate, P.R. and A.B. Pandit, *A review of imperative technologies for wastewater treatment I: oxidation technologies at ambient conditions.* Advances in Environmental Research, 8(3-4): p. 501-551, 2004.
77. Martinovic, S., et al., *Preparation of filter aids based on diatomites.* International Journal of Mineral Processing, 80(2-4): p. 255-260, 2006.
78. Deng, Z.Y., et al., *Effect of agglomeration on mechanical properties of porous zirconia fabricated by partial sintering.* Journal of the American Ceramic Society, 85(8): p. 1961-1965, 2002.
79. Arik, H., *Synthesis of Si_3N_4 by the carbo-thermal reduction and nitridation of diatomite.* Journal of the European Ceramic Society, 23(12): p. 2005-2014, 2003.
80. Stoermer, F. and P.J. Smol, *The diatoms: applications for the environmental and earth sciences*. Cambridge: Cambridge University Press, 1991.
81. Hadjar, H., et al., *Elaboration and characterisation of new mesoporous materials from diatomite and charcoal.* Microporous and Mesoporous Materials, 107(3): p. 219-226, 2008.
82. Al-Qodah, Z., et al., *Adsorption of methylene blue by acid and heat treated diatomaceous silica.* Desalination, 217(1-3): p. 212-224, 2007.
83. Al-Ghouti, M.A., et al., *Microcolumn studies of dye adsorption onto manganese oxides modified diatomite.* Journal of Hazardous Materials, 146(1-2): p. 316-327, 2007.
84. Osmanlioglu, A.E., *Natural diatomite process for removal of radioactivity from liquid waste.* Applied Radiation and Isotopes, 65(1): p. 17-20, 2007.

85. Al-Degs, Y., M.A.M. Khraisheh, and M.F. Tutunji, *Sorption of lead ions on diatomite and manganese oxides modified diatomite.* Water Research, 35(15): p. 3724-3728, 2001.
86. Sherman, J.D., *Synthetic zeolites and other microporous oxide molecular sieves.* Proceedings of the National Academy of Sciences of the United States of America, 96(7): p. 3471-3478, 1999.
87. Argauer, R.J. and G.R. Landolt, *Crystalline zeolite ZSM-5 and method of preparing the same*, United States Patent 3702886, 1972.
88. Flanigen, E.M., et al., *Silicalite, a new hydrophobic crystalline silica molecular-sieve.* Nature, 271(5645): p. 512-516, 1978.
89. Nicolaides, C.P., *A novel family of solid acid catalysts: substantially amorphous or partially crystalline zeolitic materials.* Applied Catalysis a-General, 185(2): p. 211-217, 1999.
90. Nicolaides, C.P., N.P. Sincadu, and M.S. Scurrell, *NAS (novel aluminosilicates) as catalysts for the aromatisation of propane - Studies of zinc and gallium modified zeolite-based systems having various extents of XRD crystallinity.* Catalysis Today, 71(3-4): p. 429-435, 2002.
91. Greaves, G.N., et al., *The rheology of collapsing zeolites amorphized by temperature and pressure.* Nature Materials, 2(9): p. 622-629, 2003.
92. Greaves, G.N., et al., *Zeolite collapse and polyamorphism.* Journal of Physics-Condensed Matter, 19(41), 2007.
93. Kosanovic, C., et al., *Study of structural transformations in potassium-exchanged zeolite A induced by thermal and mechanochemical treatments.* Journal of Materials Science, 32(1): p. 73-78, 1997.
94. Kosanovic, C., B. Subotic, and I. Smit, *Thermally induced phase transformations in cation-exchanged zeolites 4A, 13X and synthetic mordenite and their amorphous derivatives obtained by mechanochemical treatment.* Thermochimica Acta, 317(1): p. 25-37, 1998.
95. Kosanovic, C., et al., *Mechanochemistry of zeolites .3. Amorphization of zeolite ZSM-5 by ball-milling.* Zeolites, 15(1): p. 51-57, 1995.
96. Wang, L.M., J. Chen, and R.C. Ewing, *Radiation and thermal effects on porous and layer structured materials as getters of radionuclides.* Current Opinion in Solid State & Materials Science, 8(6): p. 405-418, 2004.
97. Triantafyllidis, K.S., et al., *Structural, compositional and acidic characteristics of nanosized amorphous or partially crystalline ZSM-5 zeolite-based materials.* Microporous and Mesoporous Materials, 75(1-2): p. 89-100, 2004.
98. Watanabe, Y., et al., *The densification of zeolite/apatite composites using a pulse electric current sintering method: A long-term assurance*

material for the disposal of radioactive waste. Journal of the European Ceramic Society, 26(4-5): p. 481-486, 2006.
99. Crittenden, B. and W.J. Thomas, *Adsorption technology and design*, p. 288: Elsevier, 1998.
100. Satterfield, C.N., *Heterogeneous catalysis in industrial practice*. New-York: Krieger Publishing Company, 1996.
101. Armor, J.N., *Do you really have a better catalyst?* Applied Catalysis a-General, 282(1-2): p. 1-4, 2005.
102. Breck, D.W., *Zeolite molecular sieves: structure, chemistry, and use*. New York: John Wiley & Sons Inc, 1974.
103. Kanamori, K., et al., *Structural formation of hybrid siloxane-based polymer monolith in confined spaces.* Journal of Separation Science, 27(10-11): p. 874-886, 2004.
104. El Haskouri, J., et al., *Silica-based powders and monoliths with bimodal pore systems.* Chemical Communications, (4): p. 330-331, 2002.
105. Li, Y.Y., et al., *The effect of the binder on the manufacture of a 5A zeolite monolith.* Powder Technology, 116(1): p. 85-96, 2001.
106. Bowes, E., *Extrusion of silica-rich solids*, United States Patent 4582815, 1986.
107. Bowes, E., *Catalytic dewaxing process using binder-free catalyst*, United States Patent 4872968, 1989.
108. Verduijn, J.P., *Process for producing substantially binder-free zeolite*, United States Patent 54607961997.
109. Van Den, B.J.M. and G.D. Mohr, *Zeolite catalyst and use for hydrocarbon conversion*, United States Patent 6977320, 2005.
110. Rauscher, M., et al., *Hydrothermal transformation of porous glass granules into ZSM-5 granules.* Microporous and Mesoporous Materials, 75(3): p. 195-202, 2004.
111. Dong, A.A., et al., *Mechanically stable zeolite monoliths with three-dimensional ordered macropores by the transformation of mesoporous silica spheres.* Advanced Materials, 14(20): p. 1506-+, 2002.
112. Tao, Y.S., H. Kanoh, and K. Kaneko, *ZSM-5 monolith of uniform mesoporous channels.* Journal of the American Chemical Society, 125(20): p. 6044-6045, 2003.
113. Tao, Y., H. Kanoh, and K. Kaneko, *Synthesis of mesoporous zeolite*, United States Patent 6998104, 2006.
114. Lee, Y.J., et al., *Synthesis of large monolithic zeolite foams with variable macropore architectures.* Advanced Materials, 13(16): p. 1259-1263, 2001.
115. Yoon, K.-B., et al., *Method of the preparation of macroporous foam comprising zeolite or zeotype material*, United States Patent 6777364, 2004.

116. Tong, Y.C., et al., *Synthesis of monolithic zeolite beta with hierarchical porosity using carbon as a transitional template.* Chemistry of Materials, 18(18): p. 4218-4220, 2006.
117. Huerta, L., et al., *Silica-based macrocellular foam monoliths with hierarchical trimodal pore systems.* Solid State Sciences, 7(4): p. 405-414, 2005.
118. Zhang, B.J., S.A. Davis, and S. Mann, *Starch gel templating of spongelike macroporous silicalite monoliths and mesoporous films.* Chemistry of Materials, 14(3): p. 1369-1375, 2002.
119. Maekawa, H., et al., *Meso/macroporous inorganic oxide monoliths from polymer foams.* Advanced Materials, 15(7-8): p. 591-596, 2003.
120. Morales, J.M., et al., *Scale-up low-cost synthesis of bimodal mesoporous silicas.* Solid State Sciences, 7(4): p. 415-421, 2005.
121. Lee, J., et al., *Simple synthesis of hierarchically ordered mesocellular mesoporous silica materials hosting crosslinked enzyme aggregates.* Small, 1(7): p. 744-753, 2005.
122. Kuang, D.B., T. Brezesinski, and B. Smarsly, *Hierarchical porous silica materials with a trimodal pore system using surfactant templates.* Journal of the American Chemical Society, 126(34): p. 10534-10535, 2004.
123. Sen, T., et al., *One-pot synthesis of hierarchically ordered porous-silica materials with three orders of length scale.* Angewandte Chemie-International Edition, 42(38): p. 4649-4653, 2003.
124. Smatt, J.H., S. Schunk, and M. Linden, *Versatile double-templating synthesis route to silica monoliths exhibiting a multimodal hierarchical porosity.* Chemistry of Materials, 15(12): p. 2354-2361, 2003.
125. Liang, C.D., S. Dai, and G. Guiochon, *Use of gel-casting to prepare HPLC monolithic silica columns with uniform mesopores and tunable macrochannels.* Chemical Communications, (22): p. 2680-2681, 2002.
126. Ishizuka, N., et al., *Designing monolithic double-pore silica for high-speed liquid chromatography.* Journal of Chromatography A, 797(1-2): p. 133-137, 1998.
127. Viswanathan, V., et al., *Challenges and advances in nanocomposite processing techniques.* Materials Science & Engineering R-Reports, 54(5-6): p. 121-285, 2006.
128. Munir, Z.A., U. Anselmi-Tamburini, and M. Ohyanagi, *The effect of electric field and pressure on the synthesis and consolidation of materials: A review of the spark plasma sintering method.* Journal of Materials Science, 41(3): p. 763-777, 2006.
129. Inoue, K., *Apparatus for electrically sintering discrete bodies*, United States Patent 3250892, 1966.

130. Inoue, K., *Electric-discharge sintering*, United States Patent 3241956, 1966.
131. Shen, Z. and M. Nygren, *Microstructural prototyping of ceramics by kinetic engineering: Applications of spark plasma sintering.* Chemical Record, 5(3): p. 173-184, 2005.
132. Oh, S.T., et al., *Strengthening of porous alumina by pulse electric current sintering and nanocomposite processing.* Journal of the American Ceramic Society, 83(5): p. 1314-1316, 2000.
133. Wang, K., et al., *Study on fabrication and mechanism in of porous metals by spark plasma sintering.* Journal of Materials Science, 42(1): p. 302-306, 2007.
134. Zhang, F.M., et al., *Spark plasma sintering of macroporous calcium phosphate scaffolds from nanocrystalline powders.* Journal of the European Ceramic Society, 28(3): p. 539-545, 2008.
135. Berglund, R.N. and B.Y.H. Liu, *Generation of monodisperse aerosol standards.* Environmental Science & Technology, 7(2): p. 147-153, 1973.
136. TSI-Incorporated, *Model 3450 Vibrating Orifice Aerosol Generator*. Instruction Manual. Shoreview, 2002.
137. Delhez, R., et al., *Crystal imperfection broadening and peak shape in the Rietveld method*. IUCr Monographs on crystallography 5, ed. R.A. Young: Oxford University Press, 1993.
138. Balzar, D., et al., *Size-strain line-broadening analysis of the ceria round-robin sample.* Journal of Applied Crystallography, 37: p. 911-924, 2004.
139. Rodríguez-Carvajal, J., *Recent developments of the program FullProf.* Commission on Powder Diffraction (IUCr) Newsletter, 26: p. 12-19, 2001.
140. van Koningsveld, H., J.C. Jansen, and H. van Bekkum, *The monoclinic framework structure of zeolite H-ZSM-5 - Comparison with the orthorhombic framework of as-synthesized ZSM-5.* Zeolites, 10(4): p. 235-242, 1990.
141. Walker, W.J. and J.S. Reed, *Green testing of pressed compacts.* Ceram. Eng. Sci. Proc., 14(11-12): p. 43-57, 1993.
142. Timoshenko, S.P. and J.N. Goodier, *Theory of elasticity*. NY: McGraw-Hill, 1970.
143. Ravikovitch, P.I. and A.V. Neimark, *Characterization of micro- and mesoporosity in SBA-15 materials from adsorption data by the NLDFT method.* Journal of Physical Chemistry B, 105(29): p. 6817-6823, 2001.
144. Ring, T.A., *Ch. 17*, in *Fundamentals of ceramic powder processing and synthesis*. San Diego: Academic Press. 1996.

145. Wu, J.L., Y.S. Yang, and J.H. Lin, *Advanced tertiary treatment of municipal wastewater using raw and modified diatomite.* Journal of Hazardous Materials, 127(1-3): p. 196-203, 2005.
146. Hurst, W.E., *Replacing food grade celite media with AW celite NF media in CGMP pharmaceutical processes*, in *Technical Note*. 2004, Advanced Mineral Corporation.
147. German, R.M., *Sintering theory and practice*. New York: John Wiley & Sons, 1996.
148. Wu, D., J. Zhou, and Y. Li, *Mechanical strength of solid catalysts: Recent developments and future prospects.* AIChE Journal, 53(10): p. 2618, 2007.
149. Mandzy, N., E. Grulke, and T. Druffel, *Breakage of TiO_2 agglomerates in electrostatically stabilized aqueous dispersions.* Powder Technology, 160(2): p. 121-126, 2005.